

**DESIGN AND MEASUREMENTS OF A
MICROWAVE CAVITY AND COUPLER FOR A
KLYSTRON TEST STAND**

**A Thesis Submitted to
the Graduate School of Engineering and Sciences of
İzmir Institute of Technology
in Partial Fulfillment of the Requirements for the Degree of**

MASTER OF SCIENCE

in Electronics and Communication Engineering

**by
Ashhan ÇAĞLAR**

**July 2019
İZMİR**

We approve the thesis of **Aslıhan ÇAĞLAR**

Examining Committee Members:

Asst. Prof. Dr. Fatih YAMAN
Department of Electrical-Electronics Engineering
İzmir Institute of Technology

Prof. Dr. M. Salih DİNLEYİCİ
Department of Electrical-Electronics Engineering
İzmir Institute of Technology

Prof. Dr. V. Erkan ÖZCAN
Department of Physics
Boğaziçi University

18 July 2019

Asst. Prof. Dr. Fatih YAMAN
Supervisor, Department of Electrical and Electronics Engineering
İzmir Institute of Technology

Prof. Dr. Enver TATLICIOĞLU
Head of the Department of
Electrical and Electronics Engineering

Prof. Dr. Aysun SOFUOĞLU
Dean of the Graduate School of
Engineering and Sciences

I want to dedicate my thesis to Nihan AĐLAR.

ACKNOWLEDGMENTS

First of all, I am sincerely grateful to my supervisor Asst. Prof. Dr. Fatih YAMAN for his trust, suggestions and support during my master's study.

I would like to thank Prof. Dr. Erkan ÖZCAN, Assoc. Prof. Dr. Gökhan ÜNEL and Dr. Hakan ÇETİNKAYA for their guidance, suggestions and support throughout the study.

I would like to thank TUBITAK for financial support it has provided under the grant 116E221.

I would like to thank my dear friends in KAHVE Laboratory for such friendly research environments they had provided.

I would also like to thank Sinan ÖZ for helping make the mechanical design of cavity and coupler.

I would especially like to thank dear Ezgi SUNAR for her unique support and contribution, which I will never forget.

Finally, I wish to thank my great family for their love, support and trust to me.

ABSTRACT

DESIGN AND MEASUREMENTS OF A MICROWAVE CAVITY AND COUPLER FOR A KLYSTRON TEST STAND

In recent years, usage of high power in modern technologies operating at microwave frequency range has been varying in research topics such as radar, plasma science, satellite communications and particle physics. Therefore, transmission of high power from a power generator to a specific target without loss is a key point of these research fields. In accordance with this purpose, a project has been started at the Kandilli Detector, Accelerator and Instrumentation (KAHVE) Laboratory of Boğaziçi University in Turkey which name is Design, Simulation and Production of an RF Circulator and Transmission Line. The aim of the project is to build a high power RF transmission line and circulator operating at 800 MHz frequency. In order to perform this whole system after their installing, a simple pillbox cavity has been designed, simulated and fabricated. A cavity is not enough itself to test the system because an efficient high power transmission section from the RF power generator to the pillbox cavity is needed. In this regard, an input power coupler with a loop antenna has also been produced. Overall, several measurements have been performed to compare with simulation results and to determine whether the performance of the transmission line is adequate for high power applications and consistent results were obtained in accordance with the project targets.

ÖZET

KLYSTRON TEST STANDI İÇİN MİKRODALGA KOVUK VE BAĞDAŞTIRICI TASARIM VE ÖLÇÜMLERİ

Son yıllarda, mikrodalga frekans aralığında çalışan modern teknolojilerde yüksek güç kullanımı, radar, plazma bilimi, uydu iletişimi ve parçacık fiziği gibi araştırma konularında değişmektedir. Bu nedenle, bir güç üreticiden kayıpsız olarak belirli bir hedefe yüksek gücün iletilmesi, bu araştırma alanlarının kilit noktasıdır. Bu amaca uygun olarak, Türkiye’de Boğaziçi Üniversitesi Kandilli Dedektör, Hızlandırıcı ve Enstrümantasyon (KAHVE) Laboratuvarı’nda RF Sirkülatör ve İletim Hattı Tasarım, Simülasyon ve Üretim adında bir proje başlatılmıştır. Projenin amacı, 800 MHz frekansında çalışan yüksek güçlü RF iletim hattı ve sirkülatör yapmaktır. Kurulundan sonra tüm bu sistemi test etmek için basit bir hap kutusu kovuğu tasarlanmış, simüle edilmiş ve üretilmiştir. Test işlemi için sadece kovuk yeterli değildir, çünkü RF güç üreticisinden hap kutusu kovuğuna verimli bir yüksek güç aktarım bölümüne ihtiyaç vardır. Bu bakımdan, döngü anteni olan güç bağdaştırıcısı da üretilmiştir. Genel olarak, simülasyon sonuçları ile karşılaştırmak ve iletim hattının performansının yüksek güç uygulamaları için yeterli olup olmadığını belirlemek için çeşitli ölçümler yapılmış ve proje hedeflerine uygun olarak tutarlı sonuçlar elde edilmiştir.

TABLE OF CONTENTS

LIST OF FIGURES	ix
LIST OF TABLES	xii
LIST OF ABBREVIATIONS	xiii
CHAPTER 1. INTRODUCTION	1
CHAPTER 2. THEORY	9
2.1. Fundamental Equations	9
2.2. Circular Waveguide	11
2.2.1. TE Mode	14
2.2.2. TM Mode	17
2.3. Cylindrical Pillbox Cavity	18
2.4. Quality Factor	20
2.5. Transmission Line Theory and Scattering Parameters.....	23
2.6. Input Power Couplers	27
2.7. Computational Electromagnetics Methods.....	29
CHAPTER 3. DESIGN AND FABRICATION OF THE PILLBOX CAVITY AND INPUT POWER COUPLER	33
3.1. Design of Input Power Coupler	33
3.2. Design of Pillbox Cavity	35
3.3. Fabrication of Pillbox Cavity and Input Power Coupler.....	39
CHAPTER 4. QUALITY FACTOR MEASUREMENTS OF PILLBOX CAVITY ..	45
4.1. Measurements of Quality Factor	45
4.1.1. Reflection-Type Measurement at Critical Coupling	46
4.1.2. Transmission Type Measurement.....	48
4.1.2.1. Experimental Setup 1	51
4.1.2.2. Experimental Setup 2	52
4.1.2.3. Experimental Setup 3	53

4.1.2.4. Experimental Setup 4	54
4.1.2.5. Experimental Setup 5	55
4.2. Power Measurement of the System	56
CHAPTER 5. CONCLUSION	62
REFERENCES	66

LIST OF FIGURES

<u>Figure</u>	<u>Page</u>
Figure 1.1. Wideröe Linac (Source: Gerigk, 2011)	1
Figure 1.2. The chart of frequency vs. particle velocity (Source: Padamsee, 2015) ..	2
Figure 1.3. Quarter-wave resonators (Source: Jensen, 2018)	3
Figure 1.4. Half-wave resonators (Source: Jensen, 2018)	4
Figure 1.5. Single spoke cavities (Source: Jensen, 2018)	4
Figure 1.6. Evolution of particle accelerator cavity	5
Figure 1.7. Block diagram of the high power RF system for an accelerator (Source: Carter, 2011)	5
Figure 1.8. The general view of RF Circulator and Transmission Line Project	7
Figure 2.1. Geometry of a cylindrical waveguide	12
Figure 2.2. Geometry of a pillbox cavity	18
Figure 2.3. A parallel RLC circuit	21
Figure 2.4. A transmission line connected to parallel RLC circuit	23
Figure 2.5. Voltage and current definition at $z = 0$ and $z = \Delta z$ (a) transmission line, (b) equivalent circuit of transmission line	24
Figure 2.6. A transmission line connected to an external circuit	25
Figure 2.7. Block diagram of 2-port network	27
Figure 2.8. The coupling types (a) slot coupling, (b) loop coupling and (c) probe coupling	28
Figure 2.9. Fabricated coupler types (a) waveguide, (b) coaxial (Source: Kumar, 2017)	29
Figure 2.10. Three meshing examples obtained by CST-MWS (a) MoM surface mesh, (b) FEM tetrahedral mesh and (c) FDTD hexahedral mesh	30
Figure 2.11. Finite elements (a) one-dimensional, (b) two-dimensional and (c) three- dimensional (Source: Sadiku, 2000)	31
Figure 3.1. Drum-like coupler designed at ESS-Bilbao (a) full view, (b) cut view (Source: Bermejo and Sordo, 2013)	33
Figure 3.2. Input power coupler at 800 MHz (a) full view, (b) cut view	34
Figure 3.3. Dimensions (mm) of the input power coupler at 800 MHz	34
Figure 3.4. Scattering parameters of the input power coupler obtained via CST- MWS	35
Figure 3.5. Pillbox cavity at 800 MHz (a) top view, (b) side view and (c) cut view ..	36

Figure 3.6. Dimensions (mm) of the pillbox cavity at 800 MHz	36
Figure 3.7. Absolute field distribution of pillbox cavity (a) electric field, (b) magnetic field	37
Figure 3.8. The resonance frequency and unloaded quality factor of pillbox cavity (a) without tuners, (b) with tuners	37
Figure 3.9. The loop antenna (a) full view, (b) cut view	38
Figure 3.10. Coupler and cavity system (a) full view, (b) cut view	38
Figure 3.11. Critical coupling results of the coupler and cavity system via the Eigenmode Solver in CST-MWS	39
Figure 3.12. Field distribution of the coupler and cavity system (a) electric field, (b) magnetic field	39
Figure 3.13. S_{11} of the coupler and cavity system obtained via the Frequency Solver in CST-MWS	40
Figure 3.14. The parts of system mount	40
Figure 3.15. Coupler cut view	41
Figure 3.16. Photograph of materials before production	41
Figure 3.17. Photograph of parts before weld	42
Figure 3.18. The picture of the produced cavity and coupler	42
Figure 3.19. Photograph of dimensions of the whole structure	43
Figure 4.1. Representation of quality factor measurements from (a) S_{11} , (b) Smith chart	47
Figure 4.2. Reflection type measurement setup	47
Figure 4.3. The reflection type measurement results (a) -3dB points of S_{11} , (b) its Smith chart representation.	48
Figure 4.4. General scheme of transmission type measurement	49
Figure 4.5. The photograph of pick-up antennas	50
Figure 4.6. Photographs of the designed 50Ω loop antennas (a) cut and full view of antenna1, (b) cut and full view of antenna2	50
Figure 4.7. Results of reflection coefficient and impedance plot for 50Ω loop antenna1 outside of the cavity	51
Figure 4.8. Results of reflection coefficient and impedance plot for 50Ω loop antenna2 outside of the cavity	51
Figure 4.9. Experimental setup 1 with pick-up antennas	52
Figure 4.10. (a) S-parameters results (b) -3dB points of S_{21} for experimental setup 1	52

Figure 4.11. Experimental setup 2 with 50Ω loop antennas.	53
Figure 4.12. (a) S-parameters results (b) -3dB points of S_{21} for experimental setup 2	53
Figure 4.13. Loaded quality factor measurement setup 3 with pick-up antenna	54
Figure 4.14. (a) S-parameters results (b) -3dB points of S_{21} for experimental setup 3	54
Figure 4.15. Loaded quality factor measurement setup 4 with 50Ω loop antennas	55
Figure 4.16. (a) S-parameters results (b) -3dB points of S_{21} for experimental setup 4	55
Figure 4.17. Loaded quality factor measurement setup 5 with pick-up antennas	56
Figure 4.18. (a) S-parameters results (b) -3dB points of S_{21} for experimental setup 5	56
Figure 4.19. (a) Measurement test stand of the cavity (b) result of the S_{11} parameter of the cavity and coupler system	57
Figure 4.20. (a) Measurement test stand of the transmission line (b) the result of the S-parameters of the transmission line	57
Figure 4.21. Power measurement test stand of the whole system.	58
Figure 4.22. (a) Attenuator test setup via VNA (b) power determination of RF power supply via spectrum analyzer	58
Figure 4.23. S-parameter results of the power measurement test setup of the whole system	60
Figure 5.1. The resonance frequency and the unloaded quality factor of pillbox cavity for $\sigma = 2.510^7 S/m$ (a) without tuners, (b) with tuners	64

LIST OF TABLES

<u>Table</u>	<u>Page</u>
Table 2.1. The values of P'_{nm} for TE modes	16
Table 2.2. The values of P_{nm} for TM modes	17
Table 2.3. Specific cases for terminated transmission line	26
Table 3.1. The comparison list of designed and measured values of the parts.	43
Table 4.1. The amount of power supplied from the RF power supply to the system.	59
Table 4.2. The results of whole system power measurement.	60
Table 5.1. The resonance frequency and the unloaded quality factor of pillbox cavity computed for $\sigma = 3.5610^7 S/m$ via the Eigenmode Solver in CST-MWS	62
Table 5.2. The S-parameter values of the input power coupler obtained via the Frequency Solver in CST-MWS	62
Table 5.3. The values of the resonance frequency and the quality factors of the cavity and coupler system obtained via the Eigenmode Solver in CST-MWS	63
Table 5.4. The S-parameters of the cavity and coupler system obtained via the Frequency Solver in CST-MWS	63
Table 5.5. The results of quality factor measurements.	64
Table 5.6. The percentage error between measured and simulated values	65

LIST OF ABBREVIATIONS

AC	Alternating Current
AKS	Advanced Krylov Subspace Method
CNC	Computer Numerical Control
CST	Computer Simulation Technology
DC	Direct Current
DTL	Dirft Tube Linear
EM	Electromagnetic
FDTD	Finite Difference Time Domain
FIT	Finite Integration Technique
HWR	Half-Wave Resonator
IL	Insertion Loss
IFBW	Intermediate Frequency Bandwidth
JDM	Jacobi Davidson Method
KAHVE	Kandilli Detector, Accelerator and Instrumentation Laboratory
MoM	Method of Moments
MWS	Microwave Studio
QWR	Quarture-Wave Resonator
RF	Radio Frequency
RL	Return Loss
RLC	Resistor,Inductor,Capacitor
S-parameter	Scattering parameter
TE	Transverse Electric
TEM	Transverse Electromagnetic
TM	Transverse Magnetic
TUBITAK	Scientific and Technological Research Council of Turkey
UHF	Ultra High Frequency
VHF	Very High Frequency
VNA	Vector Network Analyzer

CHAPTER 1

INTRODUCTION

Progress in particle physics has been driven by progress in particle accelerators. Various kinds of particle accelerators should have been invented for discovering new particles. These differentiated accelerators can be divided into two groups as electrostatic and electromagnetic in accordance with whether the current of the power generator is direct (DC) or alternating (AC). Concerning that earlier particle accelerators were produced by electrostatic power supplies but there have been several limitations such as the size of the generators, discharging or electrical breakdown. Within the time for the invention of higher energetic particles, a new generation of accelerators have been born by using electromagnetic fields, which is called Radio Frequency (RF) accelerators (Hinterberger, 2006; Wangler, 2008).

Rolf Wideröe produced the first RF accelerator in 1928 by using a series of metal drift tubes connected to the alternating current source as shown in Figure 1.1. The working principle of the structure is to load two successive drift tubes with opposite electrical charges and to form an electric field that accelerates particles between two drift tubes, which is called “*acceleration gap*”. However, particles can face an accelerating or decelerating force based on changing polarity of the source. In order to prevent this effect, the time particles take to travel from one drift tube to the next drift tube should be half of the RF source period. Also, the lengths of the drift tubes should be increased at each acceleration gap to ensure synchronization between electric field and particles.

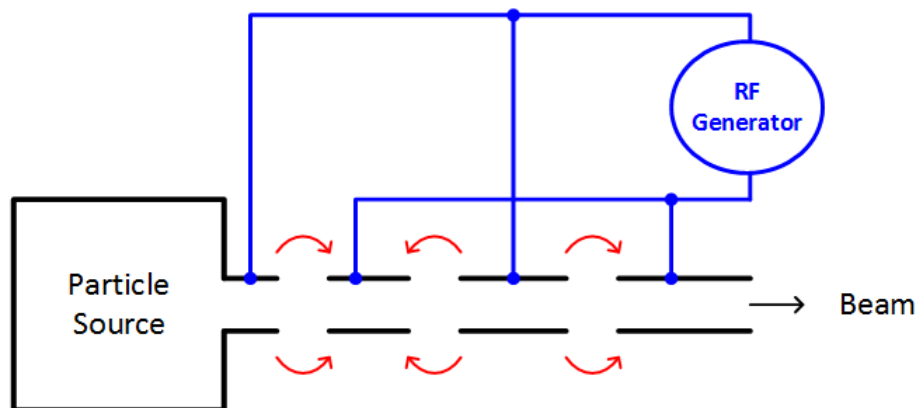


Figure 1.1. Wideröe Linac (Source: Gerigk, 2011)

The speed of light particles, such as electrons, increases very rapidly compared to heavy ions. Hence very long drift tubes or high-frequency power supplies are needed to ensure the condition of synchronism for Wideröe type accelerators. However, the structure behaves like an antenna at high frequency. To prevent this radiation, in 1947, Luis Alvarez developed a drift tube linear accelerator (DTL) by placing drift tubes into a closed cylindrical structure by providing synchronization conditions (Gerigk, 2011; Vretenar, 2016).

One of the fundamental components of any RF accelerator structure is its accelerating cavities. There are many types of accelerating cavities for various applications. They can be examined in three groups depending on the particle velocity or the type of electromagnetic field to be used to accelerate the particles in the cavity. The velocity of a particle is determined by beta which indicates how close it is to the speed of light (their relationship is defined as $\beta = \frac{v}{c}$ where c is the speed of light and v is the speed of particle in the cavity). In this context, RF cavities can be grouped as high beta, medium beta and low beta or according to electromagnetic modes are defined as transverse electric (TE), transverse magnetic (TM) and transverse electromagnetic (TEM) (Gerigk, 2011; Padamsee, 2015). Figure 1.2 shows some practical examples of structures according to frequency concerning particle velocity.

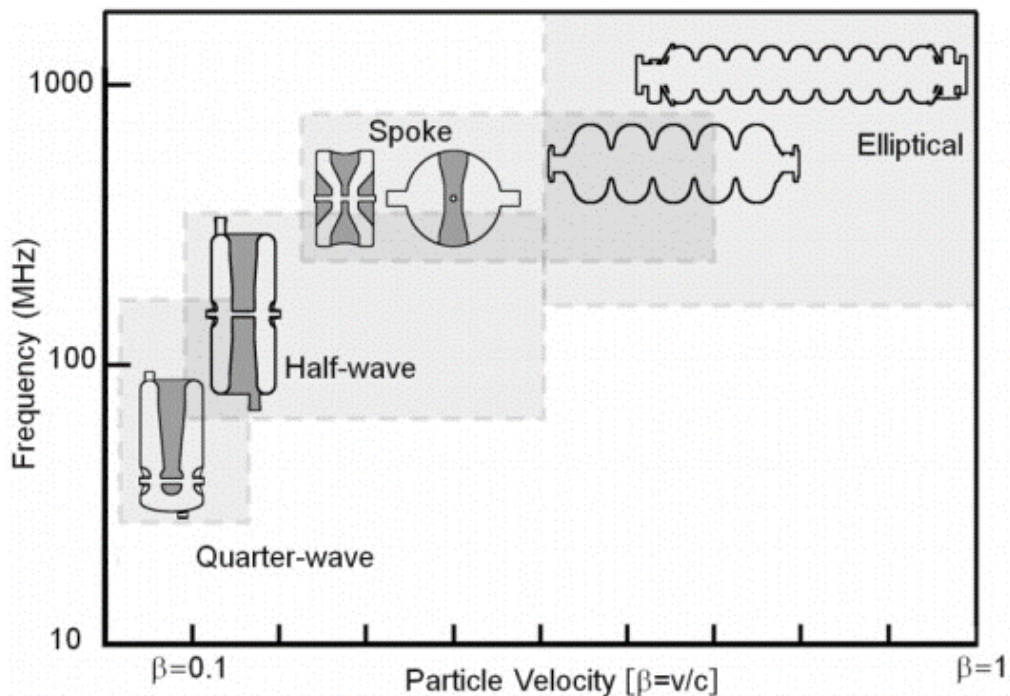


Figure 1.2. The chart of frequency vs. particle velocity (Source: Padamsee, 2015)

When particles are accelerated by using TE and TM modes at low frequencies, cavity sizes become excessively large because of dependence on the transverse dimensions. Here, one can take advantage of TEM mode cavities in which its length determines RF frequency (Jensen, 2018). TEM mode resonators can be grouped as quarter wave resonator (QWR) and half wave resonator (HWR) in which behave like a transmission line. These structures are also called as low velocity or low beta cavity which has used for acceleration of heavy ions.

The operating frequency of QWR should be range between 50-160 MHz to achieve suitable dimensions of the structure or β should be varying from 0.001 to 0.2. In order to form QWR, the top side of the inner conductor is ended with a short circuit and the other side is terminated with an open circuit. Some examples of the structure are as seen in Figure 1.3. The maximum electric field is obtained at $\frac{\lambda}{4}$, where λ is the wavelength related to the operating frequency, in this regard, the beam pipe is positioned here. The orientation of particles by the beam pipe is not proper due to asymmetrical fields in the resonator and mechanical vibration may be caused owing to their massive body. To overcome these limitations, gap shaping has been used to prevent the deviation of electromagnetic fields and the other problem has been solved by using fast tuners (Padamsee, 2015).



Figure 1.3. Quarter-wave resonators (Source: Jensen, 2018)

A half wave resonator (HWR) has the maximum electric field at $\frac{\lambda}{2}$, so the beam tube is positioned there and both ends of the inner conductor are terminated by the short circuit to form HWR, owing to this symmetry, the beam steering is better than QWR. The operating frequency of HWR ranges between 140-325 MHz and the particle velocity (β) varies from 0.1 to 0.5. Thus, these structures have smaller dimensions compared to QWR, which means that mechanical vibration properties are improved. Some practical

examples of structures are shown in Figure 1.4.

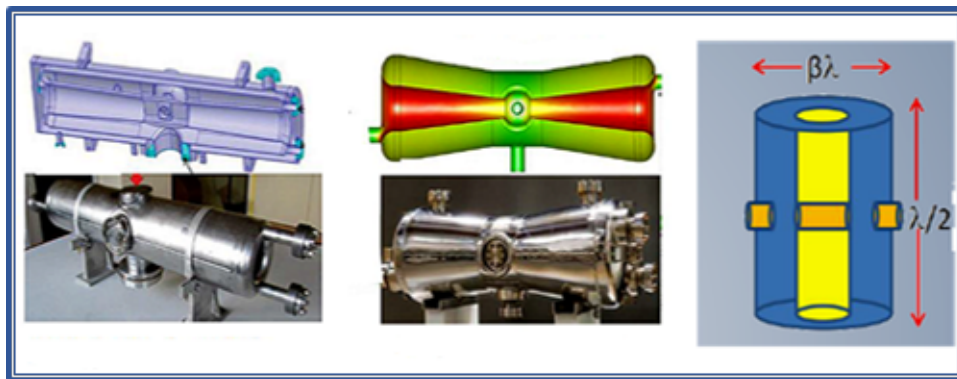


Figure 1.4. Half-wave resonators (Source: Jensen, 2018)

Another TEM mode cavity is a spoke resonator, which consists of one or more than one spoke elements. Here, the spokes are made by using an elliptical shape which is perpendicular to the beam tube, with a half wavelength transmission line. The spoke resonators are also called medium beta structures with the particle velocity and the operating frequency ranging from 0.15 to 0.7 and from 350 MHz to 700 MHz, respectively. Figure 1.5 shows some realized examples of a spoke cavity.

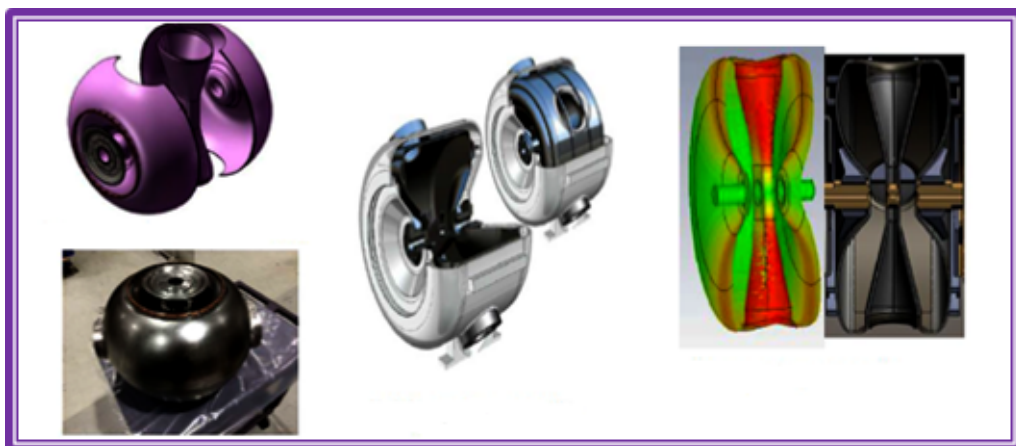


Figure 1.5. Single spoke cavities (Source: Jensen, 2018)

The elliptic or high beta cavities, as shown in Figure 1.6, are derived by softening hard corners of a cylindrical resonator and adding beam pipes to the structure. TM_{010} mode is used to accelerate particles in high beta structures which ensures the electric field is at acceleration direction and the magnetic field rotates around this direction. The elliptical cavities have a wide application area with a frequency range between 350 MHz and 4

GHz. Also, the particle velocity (β) should vary between 0.5 and 1 to obtain mechanically stable structure. Multi-cell elliptic cavities have used to get higher speeds by combining cells consecutively. In this context, an efficient acceleration is accomplished by providing an equal electric field to charged particles passing each cell in half of the RF period for high beta structures. Therefore, the design of accelerator cavities can be varied according to their intended usage or the particle to be accelerated (Padamsee, 2015).

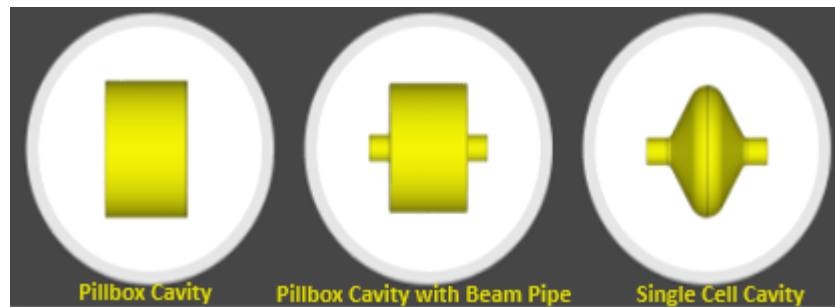


Figure 1.6. Evolution of particle accelerator cavity

The rapid development of devices and systems operating at ultra high frequency (UHF) and very high frequency (VHF) bands continuously are increasing the importance of implementation of high-power high-frequency techniques. These techniques have been used in applications such as accelerators, radar systems, heaters, defense and space technologies. Hence, a high power microwave source is one of the essential parts for all these devices and systems. Figure 1.7 shows a generic RF power system for accelerators.

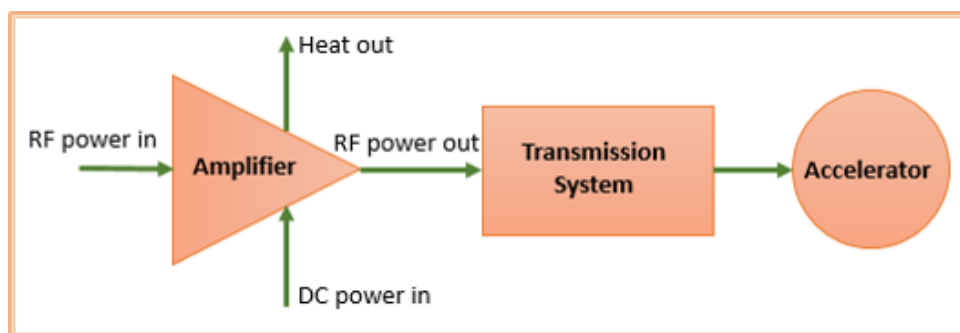


Figure 1.7. Block diagram of the high power RF system for an accelerator (Source: Carter, 2011)

The RF sources can be grouped as vacuum tubes, tube types, solid-state and single transistor according to their structure, operating principle, frequency range, efficiency or gain (Carter, 2011). Klystrons are a vacuum-tube power source operating at microwave

frequencies, which consists of three separate sections such as the gun section, RF interaction section and collector section. This power source is an indispensable device for particle accelerators. The operation principle of klystrons is based on velocity and current modulation. To understand these terms, the sections of the klystrons can be examined in detail. In this context, in the gun section, the cathode is heated to produce an electron beam. Then these released electrons are accelerated by applying DC voltage before arriving at the interaction region. This region can consist of two or more than two cavities according to the necessity of gain, bandwidth or efficiency. When the electron beam passes through the first cavity which is supplied by an external RF power source, the electron beams are accelerated or decelerated by the electromagnetic fields as they travel in the drift region. These variations in the velocity of the electrons compose the bunch and are called velocity modulation. When the beam passes through a series of output cavities, the density of the electrons increases over time. This density variation is called current modulation (Liao, 1989; Tenenbaum, 2003b). Then, this loaded-beam transfers its kinetic energy to the RF fields at the deceleration cycle in the output cavity and the residual beam is moved to the collector section as well. Then the obtained RF field is extracted from klystron by using coupling probes or waveguides to convey to the transmission system that consists of parts such as couplers, windows, circulators, etc. The main idea behind this system is to transmit power obtained from an RF source to an accelerator by minimizing dissipated power.

In this regard, it is worth noting that conveying produced power is as important as providing high power. The high power RF system is widely used in the world and key to the existence of technological development. These devices are not being produced in Turkey due to a lack of know-how. Hence, this creates an external dependency for the high-tech needs of our country in transferring power from RF power sources and absorbing any reflected power. The way to get rid of this dependence is the high-cost RF transmission line components can be produced with local facilities and the required knowledge about these technologies can be obtained. In this context, the RF circulator and transmission line project has been started at the Kandilli Detector, Accelerator and Instrumentation (KAHVE) Laboratory of Boğaziçi University in May 2017 supported by the Scientific and Technological Research Council of Turkey (TUBITAK) under the grant 116E221 (Çetinkaya et al., 2018). A high power RF transmission line and circulator operating at 800 MHz have been designed, built and constructed as shown in Figure 1.8 and this project was completed successfully in April 2019 in line with the desired targets.

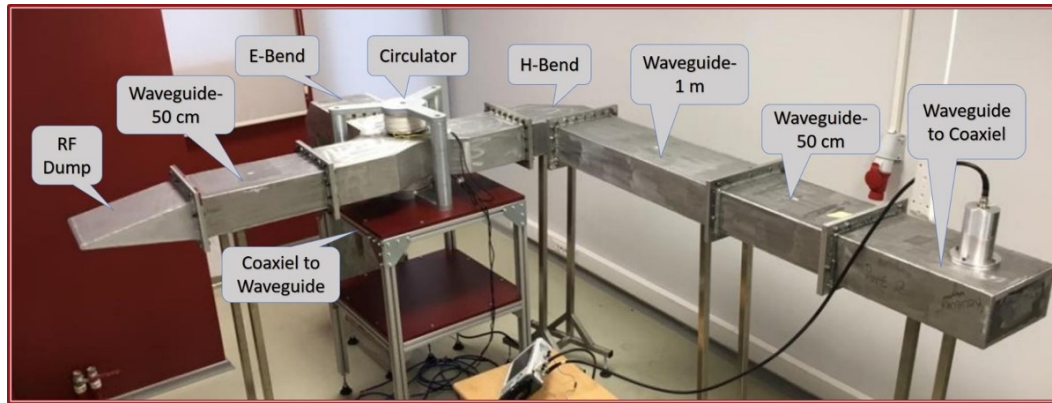


Figure 1.8. The general view of RF Circulator and Transmission Line Project

A high power transmission line can be examined in two groups as coaxial and waveguide. For this project, the waveguide type transmission line is chosen because of fewer power losses, ease of production and high power transmission capacity (Cooper, 1992). Considering these features, all waveguides are designed and manufactured at the operating frequency range between 640 MHz to 960 MHz in accordance with the Electronic Industries Alliance standard. The constructed transmission line consists of a coaxial-waveguide converter, rectangular waveguides, an E and an H bend, a 3-port waveguide circulator, a waveguide-coaxial converter and a pillbox cavity with an input power coupler. Due to the transmission line preference and the coaxial output of the power supply, the coaxial-waveguide and the waveguide-coaxial converters are used to transmit power from the power supply unit to the transmission line and to transfer power from the transmission line to the cavity. In this study, one of the most essential parts of the transmission line is the circulator which is a three-port passive device. The circulator is used to eliminate the reflected power from the pillbox cavity by conveying it on the RF dump in order to protect the power source. The last parts of the transmission line are the E and H bends which are used to channel to the electromagnetic waves in 90 degrees turns.

The particular focus of this thesis is the design, construction and measurement of the pillbox cavity and the power coupler at 800 MHz. In this context, to analyze the pillbox cavity, which forms a basis of elliptic cavities, electromagnetic background information will be reviewed in the second chapter. Also, quality factor is described to assess the cavity performance. In order to understand the measurement section, transmission line theory and S-parameters will be mentioned. The properties of the input power couplers that transmit power to the cavity will be summarized. Computational electromagnetics methods will also be introduced briefly in this chapter.

In the third chapter, simulation results will be shown and the fabrication stage of the cavity and the coupler will be discussed.

Chapter four is dedicated to the measurement techniques and measurement results will be shown.

In the final chapter, the results from the measurement section will be summarized and a discussion of my experiences during the project will be presented.

CHAPTER 2

THEORY

The solution of Maxwell's wave equation with boundary conditions will be the first topic in this chapter to understand what kind EM configurations are formed in a medium or which structures can be used as a particle accelerator. Firstly, cylindrical waveguides will be analyzed to understand fundamental behaviors of a pillbox cavity. Afterward, quality factor parameter will also be defined to specify performance of the cavity. In order to comprehend the next chapter, transmission line theory, S-parameters and input power couplers will be mentioned. The last section of this chapter is dedicated to computational electromagnetics methods.

2.1. Fundamental Equations

The electromagnetism can be expressed by using four fundamental equations that describe the behavior of electric and magnetic fields in a medium and their propagation together as a wave. These are called Maxwell's equations and their differential form is given as in the following (Pozar, 2012; Balanis, 2012):

$$\begin{aligned}\nabla \times \vec{E} &= -\frac{\partial \vec{B}}{\partial t} \\ \nabla \times \vec{H} &= \vec{J} + \frac{\partial \vec{D}}{\partial t} \\ \nabla \cdot \vec{D} &= \rho \\ \nabla \cdot \vec{B} &= 0\end{aligned}\tag{2.1}$$

Here \vec{E} , \vec{H} , \vec{D} and \vec{B} are electric field intensity, magnetic field intensity, electric flux density and magnetic flux density, respectively. Additionally, \vec{J} stands for electric current density and ρ indicates the charge density. In order to obtain the fields \vec{E} , \vec{H} , \vec{D} , \vec{B} which are generated by the sources we need constitutive relations which two of them are shown in Equation 2.2:

$$\begin{aligned}\vec{D} &= \epsilon \vec{E} \\ \vec{B} &= \mu \vec{H}\end{aligned}\tag{2.2}$$

Regarding this, the electric permittivity ϵ and the magnetic permeability μ depend on the medium and they are considered as material properties in response to the electric and

magnetic fields physical medium. These parameters can be defined in a vacuum as below:

$$\begin{aligned}\mu_0 &= 4\pi \times 10^{-7} \text{Hm}^{-1} \\ \varepsilon_0 &= \frac{1}{\mu_0 c^2} \text{Fm}^{-1}\end{aligned}\quad (2.3)$$

where c is the speed of the light in vacuum. The relative permittivity and permeability for the other materials can be calculated by using these relations $\mu_r = \frac{\mu}{\mu_0}$ and $\varepsilon_r = \frac{\varepsilon}{\varepsilon_0}$. In order to solve Equation 2.1, constitutive relations are needed as mentioned before. In this context, the other relations are defined as $\vec{J} = \vec{J}_s + \vec{J}_i$ and $\vec{J}_i = \sigma \vec{E}$ where σ is the conductivity, \vec{J}_s and \vec{J}_i are source and current densities respectively. Combining constitutive relations with electromagnetic (EM) fields for source free region ($\vec{J}_s = 0, \rho = 0, \sigma = 0$), Maxwell's equations become:

$$\begin{aligned}\nabla \times \vec{E} &= -\mu \frac{\partial \vec{H}}{\partial t} \\ \nabla \times \vec{H} &= \varepsilon \frac{\partial \vec{E}}{\partial t} \\ \nabla \cdot \vec{E} &= 0 \\ \nabla \cdot \vec{H} &= 0\end{aligned}\quad (2.4)$$

The homogenous wave equations for the electric field can be obtained by using the vector identity $\Delta \vec{A} = \nabla \cdot (\nabla \cdot \vec{A}) - \nabla \times \nabla \times \vec{A}$ according to the following steps:

$$\begin{aligned}\nabla \times \vec{E} &= -\mu \frac{\partial \vec{H}}{\partial t} \\ \nabla \times \nabla \times \vec{E} &= -\mu \frac{\partial}{\partial t} (\nabla \times \vec{H}) \\ \nabla \cdot (\nabla \cdot \vec{E}) - \Delta \vec{E} &= -\mu \frac{\partial}{\partial t} \left(\varepsilon \frac{\partial \vec{E}}{\partial t} \right) \\ \Delta \vec{E} &= \mu \varepsilon \frac{\partial^2 \vec{E}}{\partial t^2}\end{aligned}\quad (2.5)$$

here $\nabla \cdot \vec{E} = 0$ for electromagnetic (EM) fields with no source. The homogeneous wave or Helmholtz equation can be derived for the magnetic field by employing the duality theorem, as seen in Equation 2.6.

$$\Delta \vec{H} - \mu \varepsilon \frac{\partial^2 \vec{H}}{\partial t^2} = 0 \quad (2.6)$$

Vector fields in Equation 2.1 are the functions of three-dimensional spatial coordinates and time. In order to omit time dependency from the field expressions, phasor representation of EM fields can be used. The phasor form of electric and magnetic fields are

obtained by using the following steps:

$$\begin{aligned}
\nabla \times \vec{E}(x, y, z, t) + \mu \frac{\partial \vec{H}(x, y, z, t)}{\partial t} &= 0 \\
\nabla \times \operatorname{Re}\{\vec{E}(x, y, z) e^{j\omega t}\} + \frac{\partial}{\partial t} \operatorname{Re}\{\mu \vec{H}(x, y, z) e^{j\omega t}\} &= 0 \\
\operatorname{Re}\{\nabla \times \vec{E}(x, y, z) e^{j\omega t}\} + \operatorname{Re}\left\{\mu \vec{H}(x, y, z) \frac{\partial}{\partial t} e^{j\omega t}\right\} &= 0 \\
\operatorname{Re}\left\{\left[\nabla \times \vec{E}(x, y, z) + j\omega\mu \vec{H}(x, y, z)\right] e^{j\omega t}\right\} &= 0 \\
\nabla \times \vec{E}(x, y, z) + j\omega\mu \vec{H}(x, y, z) &= 0
\end{aligned} \tag{2.7}$$

As shown in Equation 2.7, phasor transform effects partial derivative due to $e^{j\omega t}$ term, accordingly, non-homogeneous Helmholtz equations can be written as:

$$\begin{aligned}
\Delta \vec{E} + k^2 \vec{E} &= \nabla(\rho/\varepsilon) + j\omega\mu \vec{J}_s \\
\Delta \vec{H} + k^2 \vec{H} &= \nabla \times \vec{J}_s
\end{aligned} \tag{2.8}$$

where $k = \sqrt{\omega^2\mu\varepsilon - j\omega\mu\sigma}$ is called wave number and ω is angular frequency. When EM problems are solved by depending on boundary conditions of different types of geometries including sources, it is convenient to start solution by considering source free region. By inserting these conditions in the Equation 2.8, homogeneous Helmholtz equations are obtained as below:

$$\begin{aligned}
\Delta \vec{E} + k^2 \vec{E} &= 0 \\
\Delta \vec{H} + k^2 \vec{H} &= 0
\end{aligned} \tag{2.9}$$

where $k = \omega\sqrt{\varepsilon\mu}$ is wave number for the lossless medium. Helmholtz equations can be solved by using the separation of variables in different coordinate systems such as cartesian, cylindrical and spherical for the corresponding boundary conditions (Wolski, 2015). This method guarantees linear superposition, which means decomposition each dimension that has one specific solution which satisfies boundary conditions and Helmholtz equations. After multiplications of separated solutions for each dimension, the general solution can be obtained summation of them. Accordingly, the solution of Helmholtz equations are in the form of plane waves.

2.2. Circular Waveguide

Consider an infinitely long circular waveguide in the z-direction with a radius of “ a ” filled with a particular material of permittivity ε and permeability μ as shown in Figure 2.1. We also assume that the waveguide walls are a perfect conductor ($\sigma \rightarrow \infty$).

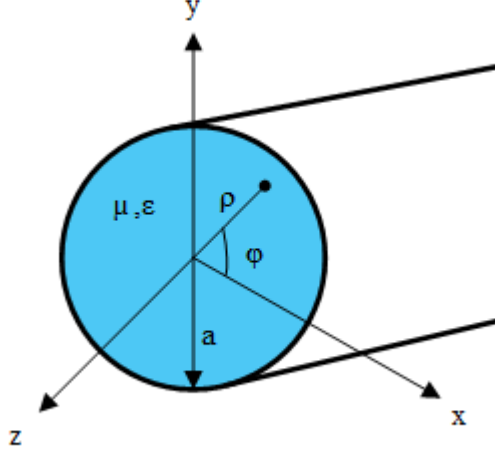


Figure 2.1. Geometry of a cylindrical waveguide

To analyze the electric and magnetic field configurations for these structures, the corresponding wave equation has to be solved in cylindrical coordinates. There are three sets of solutions for the plane waves such as transverse electric (TE), transverse magnetic (TM) and transverse electromagnetic (TEM). However, the TEM waves cannot propagate inside of a single conductor such as waveguide (Gerigk, 2013a). Hence, only the TE and TM modes will be illustrated in this section. Electric and magnetic fields can be defined in cylindrical coordinates as:

$$\begin{aligned}\vec{E}(\rho, \phi, z) &= E_\rho(\rho, \phi) e^{-j\beta z} \hat{\rho} + E_\phi(\rho, \phi) e^{-j\beta z} \hat{\phi} + E_z(\rho, \phi) e^{-j\beta z} \hat{z} \\ \vec{H}(\rho, \phi, z) &= H_\rho(\rho, \phi) e^{-j\beta z} \hat{\rho} + H_\phi(\rho, \phi) e^{-j\beta z} \hat{\phi} + H_z(\rho, \phi) e^{-j\beta z} \hat{z}\end{aligned}\quad (2.10)$$

In order to decompose each part of the electric and magnetic fields, the phasor representation of Maxwell curl equations can be used. At this point of the thesis, we start to derive each field representations in terms of EM fields in the propagating direction. To do this, we first write Maxwell curls equation in phasor forms.

$$\begin{aligned}\nabla \times \vec{E} &= -j\omega\mu\vec{H} \\ \nabla \times \vec{H} &= j\omega\varepsilon\vec{E}\end{aligned}\quad (2.11)$$

If another curl operation is applied to the electric field in Equation 2.11 the components of the magnetic field in the cylindrical coordinate are found as shown below:

$$\nabla \times \vec{E} = \frac{1}{\rho} \begin{pmatrix} \hat{\rho} & \rho\hat{\phi} & \hat{z} \\ \frac{\partial}{\partial\rho} & \frac{\partial}{\partial\phi} & \frac{\partial}{\partial z} \\ E_\rho & \rho E_\phi & E_z \end{pmatrix} = -j\omega\mu\vec{H}$$

$$\begin{aligned}
&= \frac{1}{\rho} \left[\frac{\partial E_z}{\partial \phi} - \frac{\partial (\rho E_\phi)}{\partial z} \right] \hat{\rho} - \frac{1}{\rho} \left[\frac{\partial E_z}{\partial \rho} - \frac{\partial E_\rho}{\partial z} \right] \rho \hat{\phi} + \frac{1}{\rho} \left[\frac{\partial (\rho E_\phi)}{\partial \rho} - \frac{\partial E_\rho}{\partial z} \right] \hat{z} = -j\omega\mu \vec{H} \\
H_\rho &= -\frac{1}{j\omega\mu} \left[\frac{1}{\rho} \frac{\partial E_z}{\partial \phi} - j\beta E_\phi \right] \\
H_\phi &= -\frac{1}{j\omega\mu} \left[j\beta E_\rho - \frac{\partial E_z}{\partial \rho} \right] \\
H_z &= -\frac{1}{j\omega\mu} \frac{1}{\rho} \left[\frac{\partial (\rho E_\phi)}{\partial \rho} - \frac{\partial E_\rho}{\partial \phi} \right]
\end{aligned} \tag{2.12}$$

Applying the same procedure for the magnetic field, then below equations are obtained:

$$\begin{aligned}
E_\rho &= -\frac{1}{j\omega\varepsilon} \left[\frac{1}{\rho} \frac{\partial H_z}{\partial \phi} - j\beta H_\phi \right] \\
E_\phi &= -\frac{1}{j\omega\varepsilon} \left[j\beta H_\rho - \frac{\partial H_z}{\partial \rho} \right] \\
E_z &= -\frac{1}{j\omega\varepsilon} \frac{1}{\rho} \left[\frac{\partial (\rho H_\phi)}{\partial \rho} - \frac{\partial H_\rho}{\partial \phi} \right]
\end{aligned} \tag{2.13}$$

The below equations are obtained by the arrangement of the H_ϕ from Equation 2.12 and E_ρ from Equation 2.13 component of the electric field.

$$H_\phi = -\frac{\beta}{\omega\mu} E_\rho + \frac{1}{j\omega\mu} \frac{\partial E_z}{\partial \rho} \tag{2.14}$$

$$E_\rho = \frac{1}{j\omega\varepsilon\rho} \frac{\partial H_z}{\partial \phi} - \frac{\beta}{\omega\varepsilon} H_\phi \tag{2.15}$$

Then, inserting Equation 2.14 into Equation 2.15, E_ρ is obtained with the following steps.

$$\begin{aligned}
E_\rho &= \frac{1}{j\omega\varepsilon\rho} \frac{\partial H_z}{\partial \phi} - \frac{\beta}{\omega\varepsilon} \left[-\frac{\beta}{\omega\mu} E_\rho + \frac{1}{j\omega\mu} \frac{\partial E_z}{\partial \rho} \right] \\
E_\rho &= \frac{1}{j\omega\varepsilon\rho} \frac{\partial H_z}{\partial \phi} + \frac{\beta^2}{\omega^2\mu\varepsilon} E_\rho - \frac{\beta}{j\omega^2\mu\varepsilon} \frac{\partial E_z}{\partial \rho} \\
E_\rho \left(\frac{\omega^2\mu\varepsilon - \beta^2}{\omega^2\mu\varepsilon} \right) &= \frac{1}{j\omega\varepsilon\rho} \frac{\partial H_z}{\partial \phi} - \frac{\beta}{j\omega^2\mu\varepsilon} \frac{\partial E_z}{\partial \rho}
\end{aligned} \tag{2.16}$$

where $k = \omega\sqrt{\mu\varepsilon}$ is the wave number and β is propagation constant. Afterwards by using k and β , the cut-off wave number is obtained as $k_c^2 = k^2 - \beta^2$. Consequently k_c is inserted into Equation 2.16 and E_ρ can be written as:

$$E_\rho \left(\frac{k_c^2}{k^2} \right) = \frac{1}{j\omega\varepsilon\rho} \frac{\partial H_z}{\partial \phi} - \frac{\beta}{jk^2} \frac{\partial E_z}{\partial \rho} \tag{2.17}$$

$$E_\rho \left(\frac{k_c^2}{k^2} \right) = \frac{1}{j\omega\varepsilon\rho} \frac{\partial H_z}{\partial \phi} - \frac{\beta}{jk^2} \frac{\partial E_z}{\partial \rho} \tag{2.18}$$

To obtain the rest of the field components in the cylindrical waveguide, the same steps can be applied. As a result, electric and magnetic fields components in cylindrical polar

coordinate in terms of propagation fields component are given as:

$$\begin{aligned}
E_\rho &= -\frac{j}{k_c^2} \left(\beta \frac{\partial E_z}{\partial \rho} + \frac{\omega \mu}{\rho} \frac{\partial H_z}{\partial \phi} \right) \\
E_\phi &= -\frac{j}{k_c^2} \left(\frac{\beta}{\rho} \frac{\partial E_z}{\partial \phi} - \omega \mu \frac{\partial H_z}{\partial \rho} \right) \\
H_\rho &= \frac{j}{k_c^2} \left(\frac{\omega \varepsilon}{\rho} \frac{\partial E_z}{\partial \phi} - \beta \frac{\partial H_z}{\partial \rho} \right) \\
H_\phi &= -\frac{j}{k_c^2} \left(\omega \varepsilon \frac{\partial E_z}{\partial \rho} + \frac{\beta}{\rho} \frac{\partial H_z}{\partial \phi} \right)
\end{aligned} \tag{2.19}$$

2.2.1. TE Mode

TE mode is called transverse electric mode means the electric field component in the propagation direction vanishes. In this study, +z direction is chosen for the EM wave propagation. To find the field distributions inside the waveguide in cylindrical coordinate systems, we first obtain H_z from the following homogeneous Helmholtz wave equation:

$$\Delta \vec{H}_z + k^2 H_z = 0 \tag{2.20}$$

where $\vec{H}_z(\rho, \phi, z) = h_z(\rho, \phi) e^{-j\beta z}$ and $\Delta = \frac{\partial^2}{\partial \rho^2} + \frac{1}{\rho} \frac{\partial}{\partial \rho} + \frac{1}{\rho^2} \frac{\partial^2}{\partial \phi^2} + \frac{\partial^2}{\partial z^2}$ is defined as Laplacian in cylindrical basis. By inserting these two expressions into Equation 2.20:

$$\left(\frac{\partial^2}{\partial \rho^2} + \frac{1}{\rho} \frac{\partial}{\partial \rho} + \frac{1}{\rho^2} \frac{\partial^2}{\partial \phi^2} + k_c^2 \right) h_z(\rho, \phi) = 0 \tag{2.21}$$

is obtained. Now we can apply the separation of variables and assume $h_z(\rho, \phi) = R(\rho) P(\phi)$ and this representation should satisfy Equation 2.21.

$$\left(\frac{\partial^2 R(\rho)}{\partial \rho^2} \right) P(\phi) + \left(\frac{1}{\rho} \frac{\partial R(\rho)}{\partial \rho} \right) P(\phi) + \frac{1}{\rho} \left(\frac{\partial^2 P(\phi)}{\partial \phi^2} \right) R(\rho) + k_c^2 R(\rho) P(\phi) = 0 \tag{2.22}$$

To separate analytical Equation 2.22 into ρ and ϕ components, we divide both sides with $R(\rho)P(\phi)$ and multiply both sides with ρ^2 which leads:

$$\frac{1}{R(\rho)} \rho \frac{d}{d\rho} \left[\rho \frac{R(\rho)}{d\rho} \right] + \rho^2 k_c^2 = -\frac{1}{P(\phi)} \frac{d^2 P(\phi)}{d\phi^2} \tag{2.23}$$

As shown in Equation 2.23, the left and right sides of the equation depend only ρ and ϕ respectively. According to the separation of variables, we can now solve each right-hand side by equating the zero. For instance, we can obtain the “ ϕ ” dependent function “ ρ ” from the solution of the following equation.

$$\frac{d^2 P(\phi)}{d\phi^2} + k_\phi^2 P(\phi) = 0 \tag{2.24}$$

Due to perfectly conducting surfaces, the electric field (E) and magnetic field (H) should satisfy $\hat{n} \times \vec{E} = 0$ and $\hat{n} \cdot \vec{H} = 0$, respectively where \hat{n} is the surface's normal vector. Here, $\phi \in (-\infty, \infty)$ and it is periodic with 2π . As a conclusion, field $(h_z(\rho, \phi))$ is a continuous function, periodic with 2π in ϕ component and k_ϕ is an integer. The general solution of Equation 2.24 can be obtained as:

$$P(\phi) = A \sin(k_\phi \phi) + B \cos(k_\phi \phi)$$

Let $k_\phi = n$ subjects to boundary conditions where $n = 0, 1, 2, \dots$ then:

$$P(\phi) = A \sin(n\phi) + B \cos(n\phi) \quad (2.25)$$

where A and B are arbitrary constants. To find the complete general solution, Equation 2.25 is inserted into Equation 2.24 and both sides are multiplied with $R(\rho)$:

$$\rho \frac{d}{d\rho} \left(\rho \frac{R(\rho)}{d\rho} \right) + [(k_c \rho)^2 - n^2] R(\rho) = 0 \quad (2.26)$$

Equation 2.26 is called Bessel differential equation. There are two linearly independent solution because of Equation 2.20.

$$\begin{aligned} R(\rho) &= C J_n(k_c \rho) + D Y_n(k_c \rho) \\ H_z(\rho) &= R(\rho) [A \cos(n\phi) + B \sin(n\phi)] e^{-j\beta z} \end{aligned} \quad (2.27)$$

where J_n and Y_n are n^{th} order Bessel functions of the first and second kinds respectively, C and D are arbitrary constants. However, $Y_n(\rho = 0)$ goes to infinite and causes singularity at field, so D should be equal to zero. Then the solution of h_z can be obtained as:

$$h_z(\rho, \phi) = [A \sin(n\phi) + B \cos(n\phi)] J_n(k_c \rho)$$

In order to obtain the cut-off wave number k_c , boundary conditions $E_\phi(\rho = a, \phi, z) = 0$ should be applied to E_ϕ .

$$E_\phi(\rho = a, \phi, z) = \frac{j\omega\mu}{k_c} [A \sin(n\phi) + B \cos(n\phi)] J_n(k_c a) = 0 \quad (2.28)$$

Also, Equation 2.28 can be ensured the following equation:

$$J_n'(k_c a) = 0 \rightarrow k_c a = P'_{nm} \rightarrow k_c = \frac{P'_{nm}}{a}$$

where P'_{nm} is m^{th} root of $J_n'(P'_{nm})$ and their values are listed in Table 2.1.

Table 2.1. The values of P'_{nm} for TE modes

$J'_n(P'_{nm})$	m=1	m=2
n=0	3.832	7.016
n=1	1.841	5.331
n=2	3.054	6.706

If the condition $J'_{nm}(P'_{nm}) = 0$ is applied, cut-off wave number can be obtained as:

$$k_{c,nm} = \frac{P'_{nm}}{a}$$

where $k_{c,nm}^2 = k^2 - \beta_{nm}^2$, then propagation constant and cut-off frequency become:

$$\beta_{nm} = \sqrt{k^2 + k_{c,nm}^2} = \sqrt{k^2 + \left(\frac{P'_{nm}}{a}\right)^2} \quad (2.29)$$

$$f_{c,nm} = \frac{k_{c,nm}}{2\pi\sqrt{\mu\epsilon}} = \frac{P'_{nm}}{2\pi a\sqrt{\mu\epsilon}}$$

Circular waveguides are one of the basic structures for RF cavities. They are used as beam pipes that allow transporting the beam to a cavity or vice versa. The behavior of EM wave propagation in a waveguide can be explained by using Equation 2.29 for instance; if $k > k_c$, β is real and the wave propagates or if $k = k_c$, this condition called as cut-off and if $k < k_c$, the wave is attenuated where k is the wave number in free space. For propagation modes $k > k_c$ can be expressed as in terms of wavelength and phase velocity, $\lambda = \frac{2\pi}{k}$ and $\lambda_g = \frac{2\pi}{\beta}$ are wavelength in free space and in waveguide respectively so if $k > k_c$, $v_p = \frac{\omega}{\beta} > \frac{\omega}{k} = \frac{1}{\sqrt{\mu_0\epsilon_0}} = c$ and $\lambda_g > \lambda$ can be obtained. As a result, phase velocities of propagation EM waves in waveguides are always greater than the speed of light. This means that waveguides cannot be used for the acceleration of the particles due to asynchronous with electric field (Degiovanni, 2018). The whole set of electric and magnetic field components are summarized below:

$$E_\rho = -\frac{j\omega\mu n}{k_c^2\rho} (A \cos(n\phi) - B \sin(n\phi)) J_n(k_c\rho) e^{-j\beta z}$$

$$E_\phi = \frac{j\omega\mu}{k_c} (A \sin(n\phi) + B \cos(n\phi)) J'_n(k_c\rho) e^{-j\beta z}$$

$$E_z = 0$$

$$H_\rho = -\frac{j\beta}{k_c} (A \sin(n\phi) + B \cos(n\phi)) J'_n(k_c\rho) e^{-j\beta z}$$

$$H_\phi = -\frac{j\beta n}{k_c^2\rho} (A \cos(n\phi) - B \sin(n\phi)) J_n(k_c\rho) e^{-j\beta z}$$

$$H_z = (A \sin(n\phi) + B \cos(n\phi)) J_n(k_c\rho) e^{-j\beta z}$$

2.2.2. TM Mode

TM mode refers to transverse magnetic field made which express the zero magnetic field in the z-direction ($H_z = 0$). In order to evaluate the whole electric and magnetic field components, the same steps can be applied, which were used to obtain TE mode components. In this case, z component of electric field that is $E_z(\rho, \phi, z) = e_z(\rho, \phi) e^{-j\beta z}$ can be inserted in wave equation and its solution is derived in similar way can be written as:

$$e_z(\rho, \phi) = [A \sin(n\phi) + B \cos(n\phi)] J_n(k_c \rho)$$

where A and B are arbitrary constants and J_n is the first kind of Bessel function. The boundary condition $E_z(\rho = a, \phi, z) = 0$ can be applied to E_z :

$$E_z(\rho = a, \phi, z) = [A \sin(n\phi) + B \cos(n\phi)] J_n(k_c a) e^{-j\beta z} = 0$$

In order to satisfy above equation, J_n should be equal to zero:

$$J_n(k_c a) = 0 \rightarrow k_c a = P_{nm} \rightarrow k_c \frac{P_{nm}}{a}$$

where P_{nm} is the m^{th} root of $J_n(P_{nm})$ and its values are listed in Table 2.2.

Table 2.2. The values of P_{nm} for TM modes

$J_n(P_{nm}) = 0$	m=1	m=2
n=0	2.405	5.520
n=1	3.832	7.016
n=2	5.135	8.417

The cut-off frequency and propagation constant can be defined as:

$$\beta_{nm} = \sqrt{k^2 - k_{c,nm}^2} = \sqrt{k^2 - (P_{nm}/a)^2}$$

$$f_{c,nm} = \frac{k_{c,nm}}{2\pi\sqrt{\mu\epsilon}} = \frac{P_{nm}}{2\pi\sqrt{\mu\epsilon}}$$

The smallest cut-off frequency is defined as “*dominant mode*”. For circular waveguides, TE_{11} mode has the smallest value as seen in Table 2.1. For TM mode $P_{01} = 2.405$ has the minimum value in Table 2.2. Hence, TM_{01} has greater value than P'_{11} , then dominant

mode in circular waveguide is the TE_{11} . For TM mode, the whole EM field components are summarized below:

$$\begin{aligned}
 E_z &= [A \sin(n\phi) + B \cos(n\phi)] J_n(k_c \rho) e^{-j\beta z} \\
 E_\rho &= -\frac{j\beta}{k_c} [A \sin(n\phi) + B \cos(n\phi)] J'_n(k_c \rho) e^{-j\beta z} \\
 E_\phi &= -\frac{j\beta n}{k_c \rho} [A \sin(n\phi) - B \cos(n\phi)] J_n(k_c \rho) e^{-j\beta z} \\
 H_z &= 0 \\
 H_\rho &= -\frac{j\omega \varepsilon n}{k_c^2 \rho} [A \cos(n\phi) - B \sin(n\phi)] J_n(k_c \rho) e^{-j\beta z} \\
 H_\phi &= -\frac{j\omega \varepsilon}{k_c} [A \sin(n\phi) - B \cos(n\phi)] J'_n(k_c \rho) e^{-j\beta z}
 \end{aligned}$$

2.3. Cylindrical Pillbox Cavity

The simplest cylindrical cavity resonator shape is the “pillbox” that can be obtained by covering two end walls of a cylindrical waveguide (Tenenbaum, 2003a). This structure has an infinite number of resonant modes and due to its basic shape, analytical solutions can be derived. With this approach, complicated RF cavity structures can be understood in a more straightforward way. Assume that a pillbox cavity has radius “ a ” and length “ d ” (as shown in Figure 2.2).

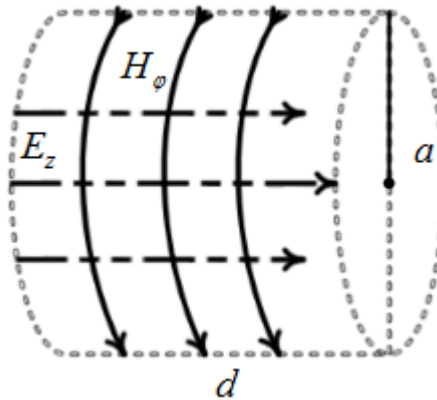


Figure 2.2. Geometry of a pillbox cavity

The aim is to find out configurations of electric and magnetic inside the cavity. There are two possible solutions as transverse electric (TE), transverse magnetic (TM) subject

to boundary conditions in a similar way to the cylindrical waveguide. However, the new boundary conditions at the end walls of the cavity ($z=0$ and $z=d$) arise standing waveforms instead of traveling waves in the solution. In the previous section, TE_{11} was found as the dominant mode for circular waveguide, in the same manner, TE_{111} is the dominant mode for pillbox cavities. To find $TE_{nm\ell}$ and $TM_{nm\ell}$ resonant modes, ϕ and ρ are transverse electric and magnetic fields of waveguide can be used as:

$$\vec{E}(\rho, \phi, z) = \vec{e}(\rho, \phi) (A^+ e^{-j\beta_{nm}z} + A^- e^{j\beta_{nm}z}) \quad (2.30)$$

where $\vec{e}(\rho, \phi)$ refers to the transverse mode variations, A^+ and A^- are the arbitrary amplitudes that + is defined as forward waves and - is backward waves. The propagation constant of TE mode was found in the former section as:

$$\beta_{nm} = \sqrt{k^2 + \left(\frac{P'_{nm}}{a}\right)^2}$$

and the propagation constant of TM mode as;

$$\beta_{nm} = \sqrt{k^2 + \left(\frac{P_{nm}}{a}\right)^2}$$

By applying boundary condition, $\vec{E}(\rho, \phi, z = 0) = 0$, $\vec{E}(\rho, \phi, z)$ can be reduced:

$$\vec{E}(\rho, \phi, z = 0) = \vec{e}(\rho, \phi) (A^+ + A^-) = 0 \quad (2.31)$$

Equation 2.31 is satisfied only if $A^+ = -A^-$. The second boundary condition, indicates $\vec{E}(\rho, \phi, z = d) = 0$, $\vec{E}(\rho, \phi)$ can be reduced:

$$\vec{E}(\rho, \phi, z) = \vec{e}(\rho, \phi) (A^+ e^{-j\beta_{nm}d} + A^- e^{j\beta_{nm}d}) = 0 \quad (2.32)$$

$$A^+ (\cos(\beta_{nm}d) - j \sin(\beta_{nm}d)) + A^- (\cos(\beta_{nm}d) + j \sin(\beta_{nm}d)) = 0. \quad (2.33)$$

$$\cos(\beta_{nm}d) (A^+ + A^-) + j \sin(\beta_{nm}d) (A^- - A^+) = 0 \quad (2.34)$$

If only $A^+ = -A^-$, Equation 2.34 cannot be fulfilled the boundary conditions accordingly. Therefore the arguments of the trigonometric functions should be selected such that,

$$\sin(\beta_{nm}d) = 0 \rightarrow \beta_{nm} = \frac{\ell\pi}{d} \text{ where } \ell = 0, 1, 2, \dots$$

The cut-off resonant frequency $f_{c,nm\ell}$ for a given TE_{nm} and TM_{nm} mode can be obtained as:

$$\text{TE resonant frequency: } f_{c,nm\ell} = \frac{c}{2\pi\sqrt{\mu_r\epsilon_r}} \sqrt{\left(\frac{\ell\pi}{d}\right)^2 + \left(\frac{P'_{nm}}{a}\right)^2}$$

$$\text{TM resonant frequency: } f_{c,nm\ell} = \frac{c}{2\pi\sqrt{\mu_r\epsilon_r}} \sqrt{\left(\frac{\ell\pi}{d}\right)^2 + \left(\frac{P_{nm}}{a}\right)^2}$$

In order to determine which fields or modes can be used in a cavity to accelerate the particles, one has to consider Lorentz Force equation:

$$\vec{F} = q \left(\vec{E} + \vec{v} \times \vec{B} \right) \quad (2.35)$$

where q and \vec{v} are charge and speed of the particle, respectively. According to Equation 2.35, $\vec{F}_e = q\vec{E}$ is the electric force with the same direction of electric field and $\vec{F}_m = q(\vec{v} \times \vec{B})$ is the magnetic force perpendicular to magnetic field and speed of charge. To calculate energy changes of a particle, work-energy relation can be used.

$$\Delta E_k = \int \vec{F} d\vec{\ell} \quad (2.36)$$

is the kinetic energy change with such that $\vec{v} = \frac{d\vec{\ell}}{dt}$.

$$\Delta E_k = q \int \vec{E} d\vec{\ell} + q \int (\vec{v} \times \vec{B}) d\vec{\ell} \quad (2.37)$$

is obtained by inserting Equation 2.35 in work-energy equation (Jensen, 2016). The magnetic field does not change the energy of a particle and only the electric field can increase the energy to accelerate particles in EM fields. Therefore, the electric field is used to accelerate particles and the magnetic field used to bend and focus particles. To supply these necessities, a special mode TM_{010} is excited and is called as an “*accelerating mode*”. Its field configuration is shown in Figure 2.2 and their equations can be written as:

$$E_z = E_0 J_0 \left(\frac{2.405\rho}{a} \right) e^{-j\omega t}$$

$$H_\phi = -j \sqrt{\frac{\epsilon_0}{\mu_0}} E_0 J_1 \left(\frac{2.405\rho}{a} \right) e^{-j\omega t}$$

then the other components are zero and resonant cut-off frequency can be defined as:

$$f_{c,010} = \frac{2.405c}{2\pi a}$$

which is independent of the cavity length according to TM_{010} mode.

2.4. Quality Factor

The quality factor is a dimensionless quantity that describes how much RF power is stored or energy is lost in the cavity and characterizes bandwidth of the cavity relative to the resonance frequency. Its formulation is defined as (Gerigk, 2013b):

$$Q = \omega_{res} \frac{\text{Stored energy in cavity}}{\text{Energy dissipated in cavity walls}} = 2\pi f_{res} \frac{W}{P_c} \quad (2.38)$$

Here, the stored energy can be calculated by using electric or magnetic fields subjected to the Ampere equation. This means that if the electric field is a maximum, the magnetic field is a minimum or vice versa. The formulation of stored energy is expressed as shown in the equation below.

$$W = \frac{\epsilon_0}{2} \iiint_V |\vec{E}|^2 dV = \frac{\mu_0}{2} \iiint_V |\vec{H}|^2 dV \quad (2.39)$$

In addition to these, power dissipation $P_c = \frac{R_s}{2} \iint_S |\vec{H}|^2 ds$, can be caused by surface resistance, $R_s = \frac{1}{\sigma\delta}$, where σ and δ are conductivity of material and skin depth respectively. The entire conductor surface cannot be used under the skin effect; so that, impedance increases because of current-flowing on a smaller section of the conductor surface and increases the losses. Consequently, higher conductivity indicates a lower loss that implies higher quality factors.

There are three different types of quality factors in terms of connection to external components. The first is the unloaded quality factor, $Q_0 = \omega_{res} \frac{W}{P_c}$, implies losses due to cavity walls or conductivity and dielectric without any external connection. The second description is an external quality factor, $Q_e = \omega_{res} \frac{W}{P_{ext}}$, is a measure of loss that can be caused by the connection of external circuits as probes, couplers, generators, etc. The last is loaded quality factor, $Q_\ell = \omega_{res} \frac{W}{P_{ext} + P_c}$, defines whole system losses. Also, their relationship with each other is interpreted as:

$$\frac{1}{Q_\ell} = \frac{1}{Q_0} + \frac{1}{Q_e} \quad (2.40)$$

Identifying values of the quality factors are one of the important subjects to characterize the RF cavity. In order to examine the effect of the quality factor in detail, the pillbox cavity can be modeled as an equivalent parallel RLC circuit (Pozar, 2012; Jensen, 2016) as shown in Figure 2.3.

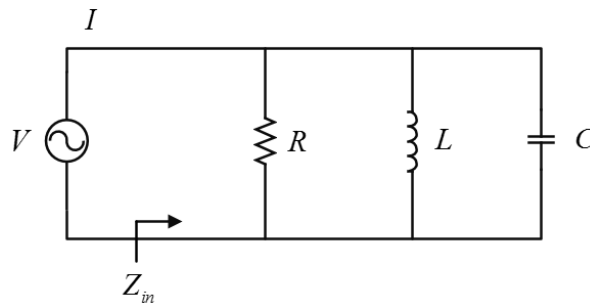


Figure 2.3. A parallel RLC circuit

Here R, L and C are passive circuit elements and they can be represented in frequency domain subject to their impedances can be written as; $Z_R = R$, $Z_L = j\omega L$ and $Z_C = \frac{1}{j\omega C}$. Z_{in} is the equivalent impedance of the circuit and is represented as:

$$Z_{in} = \left(\frac{1}{R} + \frac{1}{j\omega L} + j\omega C \right)^{-1} \quad (2.41)$$

Arranging of Equation (2.41), the below equation is obtained.

$$Z_{in} = \frac{R}{1 + jR\left(\omega C - \frac{1}{\omega L}\right)} \quad (2.42)$$

If a circuit with the elements R, L, C is at resonance state, voltage and current of the circuit are in the same phase, the complex term of impedance is zero and only active power consumption is available. Accordingly, complex term of Z_{in} is zero and the resonance angular frequency (ω_{res}) is equal to $\omega_{res} = \frac{1}{\sqrt{LC}}$. To determine Q_0 , dissipated power and storing energy in the cavity should be found. There are only ohmic power losses in the circuit at resonance, that is expressed as:

$$P_c = \frac{|V|^2}{2R} \quad (2.43)$$

Also, the electric and magnetic energy is stored in the circuit with respect to C and L at resonance. Their formulation can be represented as:

$$W_{electric} = \frac{|V|^2 C}{4} \quad (2.44)$$

$$W_{magnetic} = \frac{|V|^2}{4\omega^2 L} = \frac{|i_L|^2 L}{4} \quad (2.45)$$

Then, substituting and organizing them into unloaded quality factor equation, its formulation becomes:

$$Q_0 = \omega_{res} \frac{W}{P_c} = \frac{R}{\omega_{res} L} \quad (2.46)$$

To obtain external quality factor for parallel RLC circuit, another resistor R_L can be connected parallel to RLC circuit and $Q_e = \frac{R_L}{\omega_{res} L}$ is obtained. To find equivalent impedance of circuit, $\omega_{res} = \frac{1}{\sqrt{LC}}$ can be written as $C = \frac{1}{\omega_{res}^2 L}$ and by inserting into Equation 2.42, equivalent impedance is written as:

$$Z_{in} = \frac{R}{1 + j\frac{R}{L} \left(\frac{\omega}{\omega_{res}^2} - \frac{1}{\omega} \right)} \quad (2.47)$$

where $\frac{\omega^2 - \omega_{res}^2}{\omega_{res}^2 \omega} = \frac{(\omega - \omega_{res})(\omega + \omega_{res})}{\omega_{res}^2 \omega}$ and let assume $\omega \approx \omega_{res} \rightarrow \omega + \omega_{res} \cong 2\omega_{res}$ in order to associate with Q_0 then this equation becomes $\frac{\omega^2 - \omega_{res}^2}{\omega_{res}^2 \omega} = \frac{2}{\omega_{res}} \left(\frac{\omega - \omega_{res}}{\omega_{res}} \right)$ then, the equivalent input impedance in terms of Q_0 is obtained as below:

$$Z_{in} = \frac{R}{1 + jQ_0 2 \left(\frac{\omega - \omega_{res}}{\omega_{res}} \right)} \quad (2.48)$$

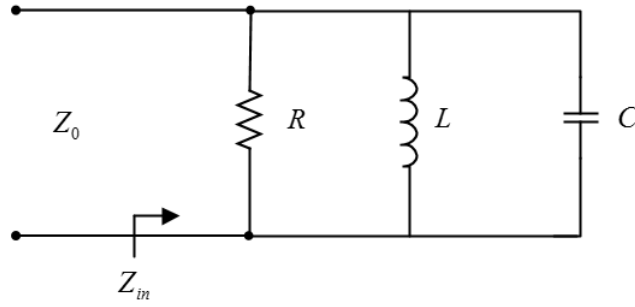


Figure 2.4. A transmission line connected to parallel RLC circuit

The transmission line should operate in a way that is compatible with the cavity to ensure maximum power transmission. According to Figure 2.4, when the cavity is critically coupled to the transmission line (Z_0 is the characteristic impedance of the transmission line), the imaginary part of the equivalent impedance is equal to zero, which means low loss or maximum power transmission. This relation is defined by using the coupling coefficient (β) and it is related to the external quality factor. To find relation between β and Q_e , resonance condition can be used in the Equation 2.48, then Z_{in} is turned into as $Z_{in} = R$, where $\omega = \omega_{res}$ and $Q_0 = \frac{R}{\omega_{res}L}$. In order to transfer power efficiently, $Z_{in} = Z_0$ should be equal each other, then $Q_e = \frac{Z_0}{\omega_{res}L} = Q_0$ is obtained for the critically coupling condition. According to Equation (2.40), loaded quality factor is equal to half of the unloaded quality factor. Coupling coefficient can be written as $\beta = \frac{Q_0}{Q_e} = \frac{R}{Z_0}$. If $\beta < 1$, $\beta = 1$ and $\beta > 1$, they are called under coupling, critical coupling and over coupling, respectively.

2.5. Transmission Line Theory and Scattering Parameters

The circuit elements such as R, L, C in a closed circuit at low frequencies are easily defined with the current which flows in the circuit. However, it is difficult to express the physical phenomenon in the circuit at the higher frequency depending on the current and it is difficult to determine the effect of the circuit element at a specific one point on the transmission line network due to scattered inductance and capacity. Current and voltage laws that are used at low frequency is not applicable to define high-frequency electrical events (Pozar, 2012; Collin, 2007). We can analyze a lossy transmission line by using equivalent circuit which is shown in the following Figure 2.5 at high frequency.

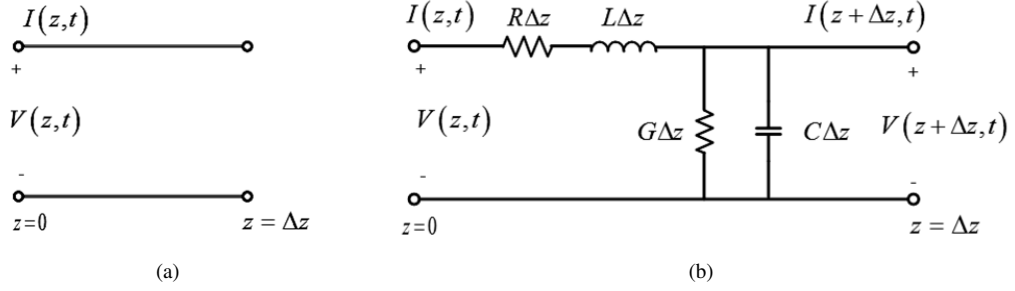


Figure 2.5. Voltage and current definition at $z = 0$ and $z = \Delta z$ (a) transmission line, (b) equivalent circuit of transmission line

Here, Δz is the length of the TL, $I(z, t)$ and $V(z, t)$ are current and voltage of TL, respectively. The Figure 2.5 is the lumped element equivalent circuit where R and L are series inductance and resistance per unit length of both conductors, their units are $\frac{\Omega}{m}$ and $\frac{F}{m}$ respectively. Also, shunt conductance can be represented as G , $\frac{S}{m}$ is its unit. C is the shunt capacitance of both conductors and its unit is $\frac{H}{m}$. Kirchhoff's current and voltage law can be applied equivalent circuit to obtain transmission line as shown in Equation 2.49 and Equation 2.50:

$$\frac{\partial V(z, t)}{\partial z} = -RI(z, t) - L\frac{\partial I(z, t)}{\partial t} \quad (2.49)$$

$$\frac{\partial I(z, t)}{\partial z} = -GV(z, t) - C\frac{\partial V(z, t)}{\partial t} \quad (2.50)$$

To simplify the above equations, the phasor domain can be used as;

$$\frac{dV(z)}{dz} = -(R + j\omega L)I(z) \quad (2.51)$$

$$\frac{dI(z)}{dz} = -(G + j\omega C)V(z) \quad (2.52)$$

Derivation of both Equations 2.51 and 2.52 with respect z , one can obtain TL equations in terms of either in voltage or in current:

$$\begin{aligned} \frac{\partial^2 V(z)}{\partial z^2} - \gamma^2 V(z) &= 0 \\ \frac{\partial^2 I(z)}{\partial z^2} - \gamma^2 I(z) &= 0 \end{aligned} \quad (2.53)$$

Here, $\gamma = \sqrt{(R + j\omega L)(G + j\omega C)} = \alpha + j\beta$ is the propagation constant where α and β are attenuation and phase constants, respectively. Solution of Equation 2.53 is expressed as:

$$V(z) = V^+ e^{-\gamma z} + V^- e^{\gamma z} \quad (2.54)$$

$$I(z) = I^+ e^{-\gamma z} + I^- e^{\gamma z} \quad (2.55)$$

where $V^+e^{-\gamma z}$ and $I^+e^{-\gamma z}$ are called voltage and current wave at $+z$ direction or incident waves, respectively and the others propagate at $-z$ direction or are called reflected waves. Substituting Equations 2.54 and 2.55 into Equation 2.51, the current wave propagates on the line is obtained in terms of voltage wave as:

$$I(z) = \frac{\gamma}{R + j\omega L} (V^+e^{-\gamma z} - V^-e^{\gamma z}) \quad (2.56)$$

Here $\frac{1}{Z_0} = \frac{\gamma}{R + j\omega L}$ can be defined by using Ohm's Law, then the characteristic impedance is represented as $Z_0 = \sqrt{\frac{R + j\omega L}{G + j\omega C}}$. Arranging voltage and current waves in terms of characteristic impedance is led to:

$$\begin{aligned} V(z) &= V_0^+e^{-\gamma z} + V_0^-e^{\gamma z} \\ I(z) &= \frac{V_0^+}{Z_0}e^{-\gamma z} - \frac{V_0^-}{Z_0}e^{\gamma z} \end{aligned} \quad (2.57)$$

In practice, it is generally desirable to transmit EM waves without loss or minimum loss. For a lossless transmission line, R and G should be equal to zero. Because R defines the loss due to finite conductivity and G represents the dielectric loss in the conductors. For a lossless line the propagation constant and characteristic impedance can be written as; $Z_0 = \sqrt{\frac{L}{C}}$ and $\gamma = \alpha + j\beta = j\omega\sqrt{LC}$ where $\alpha = 0$ and $\beta = \omega\sqrt{LC}$, respectively. Substituting these parameters into Equation 2.57:

$$\begin{aligned} V(z) &= V_0^+e^{-\beta z} + V_0^-e^{\beta z} \\ I(z) &= \frac{V_0^+}{Z_0}e^{-\beta z} - \frac{V_0^-}{Z_0}e^{\beta z} \end{aligned} \quad (2.58)$$

If a TL is terminated with a load impedance or connected to another device as shown in Figure 2.6, wave reflections can be occurred due to impedance mismatching $Z_0 \neq Z_L$. Assume that $V_0^+e^{-j\beta z}$ represents the incident wave at $z = -\ell$.

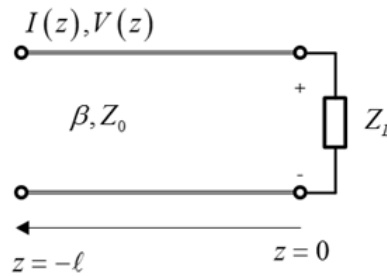


Figure 2.6. A transmission line connected to an external circuit

The total voltage and current on the line can be written as:

$$\begin{aligned} V(z) &= V_0^+e^{-\beta z} + V_0^-e^{\beta z} \\ I(z) &= \frac{V_0^+}{Z_0}e^{-\beta z} - \frac{V_0^-}{Z_0}e^{\beta z} \end{aligned} \quad (2.59)$$

To obtain total voltage and current at the load, one can put $z = 0$ in Equation 2.59:

$$\begin{aligned} V(z = 0) &= V_0^+ + V_0^- \\ I(z = 0) &= \frac{V_0^+}{Z_0} - \frac{V_0^-}{Z_0} \end{aligned} \quad (2.60)$$

Then the ratio of voltage to current gives the load impedance as:

$$Z_L = \frac{V(z = 0)}{I(z = 0)} = \frac{V_0^+ + V_0^-}{V_0^+ - V_0^-} Z_0 \quad (2.61)$$

From Equation 2.61 reflected voltage $V_0^- = \frac{Z_L - Z_0}{Z_L + Z_0} V_0^+$ can be obtained. The ratio of reflected voltage to incident voltage is called “*reflection coefficient*” and defined as $\Gamma = \frac{V_0^-}{V_0^+} = \frac{Z_L - Z_0}{Z_L + Z_0}$. For some specific cases magnitude of the reflection coefficient values are shown in the following Table 2.3.

Table 2.3. Specific cases for terminated transmission line

Open Circuit	$Z_L = \infty$	$ \Gamma = 1$
Short Circuit	$Z_L = 0$	$ \Gamma = 1$
Matched Load	$Z_L = Z_0$	$ \Gamma = 0$

This parameter expresses a measure of the impedance matched at the load connection point and determines how much power is delivered from the transmission line to the load by using the below equation.

$$P_{ave} = \underbrace{\frac{1}{2Z_0} |V_0^+|^2}_{IncidentPower} - \underbrace{\frac{1}{2Z_0} |V_0^+|^2 |\Gamma|^2}_{ReflectedPower}$$

Also, reflection coefficient can be determined by using scattering parameters that define the ratio of incident voltage wave to reflected voltage wave and N-port scattering matrix is defined as:

$$\begin{pmatrix} V_1^- \\ \vdots \\ V_N^- \end{pmatrix} = \begin{pmatrix} S_{11} & \cdots & S_{1N} \\ \vdots & \ddots & \vdots \\ S_{N1} & \cdots & S_{NN} \end{pmatrix} \begin{pmatrix} V_1^+ \\ \vdots \\ V_N^+ \end{pmatrix}$$

where $S_{ij} = \left. \frac{V_i^-}{V_j^+} \right|_{V_k^+ = 0 \text{ for } k \neq j}$ is defined as ratio of incident voltage wave V_j^+ on port to reflected wave amplitude V_i^- from port i . Two-port network is expressed as shown in Figure 2.7.

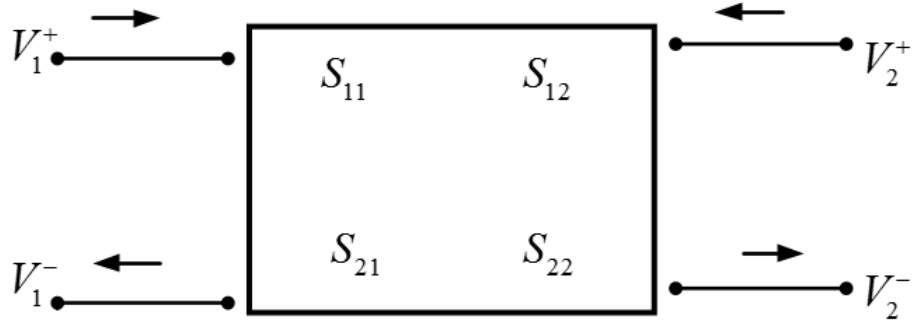


Figure 2.7. Block diagram of 2-port network

$$S_{11} = \left. \frac{V_1^-}{V_1^+} \right|_{V_2^+ = 0} \rightarrow \text{Input reflection coefficient}$$

$$S_{12} = \left. \frac{V_1^-}{V_2^+} \right|_{V_1^+ = 0} \rightarrow \text{Backward transmission coefficient}$$

$$S_{21} = \left. \frac{V_2^-}{V_1^+} \right|_{V_2^+ = 0} \rightarrow \text{Forward transmission coefficient}$$

$$S_{22} = \left. \frac{V_2^-}{V_2^+} \right|_{V_1^+ = 0} \rightarrow \text{Output reflection coefficient}$$

Moreover, the reflection coefficient can be calculated by using Return Loss equation ($RL = -20 \log |\Gamma|$) by employing positive dB value at operating frequency from reflection coefficients of S-parameter plot. In this context, if magnitude of reflection coefficient is equal to zero, return loss goes to infinity ($|\Gamma| = 0 \rightarrow RL = \infty$). This condition indicates there is no reflection. The reflected power in percent can be obtained by using equation $ReflectedPower(\%) = 100 * |\Gamma|^2$. Insertion Loss equation ($IL = -20 \log |\tau|$ where τ is transmission coefficient) can be used to find how much power is transmitted to a system. By utilizing equation $TransmittedPower(\%) = 100 * |\tau|^2$, the transmitted power in percent can be gained by using positive dB value at operating frequency from transmission coefficients of S-parameter plot.

2.6. Input Power Couplers

Power couplers can be defined as a cornerstone of transmission of RF power from a source to cavity (Nyfors et al., 2000; Alesini, 2011). In order to excite EM fields inside the cavity, slots, probes and loop antennas can be used as a part of a waveguide or a coaxial structure as shown in Figure 2.8. The power couplers can be defined as an electric

or magnetic coupling in terms of the type of stimulated fields from a transmission line or network to a cavity. Different types of couplers have advantages and disadvantages in terms of design, power handling and coupling efficiency. According to the excitation type, slots and loop antennas are employed for magnetic coupling. To excite the accelerating mode in the cavity with a slot, a waveguide coupler should be used. For coupling magnetic fields of the waveguide to the magnetic field of the cavity, either the physical size of the slot can be changed or the short circuit plane by keeping the dimensions of the slot can be changed change. Coaxial couplers can be realized with loop antennas for magnetic coupling as well. The flowing current on the loop surface generates a magnetic field and its intensity is proportional to the loop area. This field couples to the magnetic field of the desired mode that is perpendicular to the plane of the loop. Also, the coupling factor can be adjusted according to the loop's size or orientation of a short circuit plane with a constant loop's size. Probe antenna can be used in coaxial couplers subject to electric coupling. Due to the current on the coaxial inner conductor, an electric current is formed by the probe and this current is coupled with the electric field in the cavity.

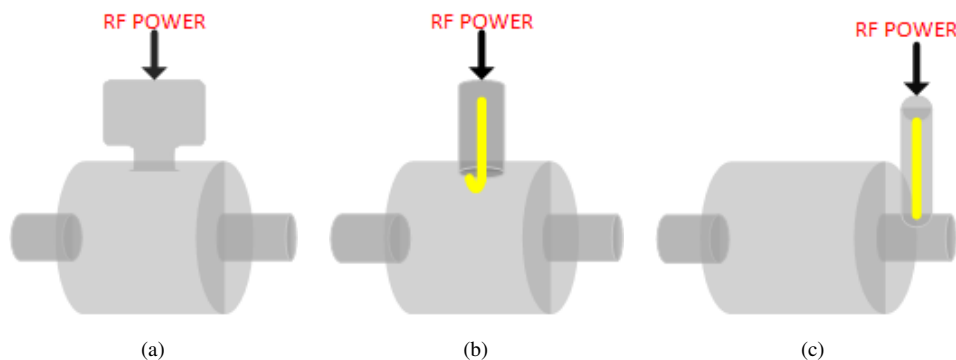


Figure 2.8. The coupling types (a) slot coupling, (b) loop coupling and (c) probe coupling

Waveguide and coaxial couplers are classified by comparing in terms of advantages or disadvantages. For example, waveguide coupler is usually used at high-frequency structures due to supporting TE and TM mode. Hence its frequency depends on the transverse dimensions of construction and is inversely proportional to the size of the structure. However, coaxial couplers can be used in lower frequency structures due to their reduced size because they use TEM mode and frequency is independent of the transverse dimension of the structure. But, waveguide type couplers do not need any transition part like coaxial couplers so that it can be designed efficiently and they cause low RF losses. Moreover, according to coupling property, waveguide couplers are more difficult matchable to

external devices in contrast to coaxial type. Typical examples of the waveguide and coaxial coupler types (Kumar, 2017) are shown in Figure 2.9.

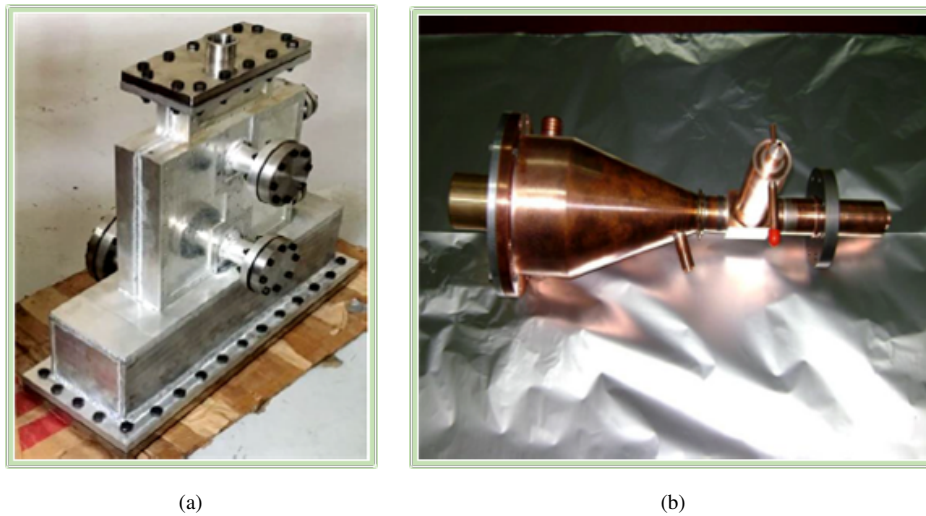


Figure 2.9. Fabricated coupler types (a) waveguide, (b) coaxial (Source: Kumar, 2017)

2.7. Computational Electromagnetics Methods

Analyzing electromagnetic fields in complicated structures or nonhomogeneous medium cannot be calculated analytically. In this respect, numerical or full-wave methods have been developed to solve these problems. The most familiar techniques are method of moments (MoM), finite difference time domain (FDTD) and finite element method (FEM). Many commercial and free electromagnetic simulation programs are based on solving Maxwell's equations in different forms of numerically. In this thesis, Computer Simulation Technology Microwave Studio (CST-MWS) is used for simulations (CST, 2018). CST-MWS offers the main four different solvers that are transient solver, frequency domain solver, integral equation solver and eigenmode solver to supply more effective solutions. Also, these solvers use finite integration technique (FIT), advanced krylov subspace method (AKS), jacobi davidson method (JDM), FEM and MoM because the programs cannot supply all different applications with a single solver. Hence, different numerical methods are selected and integrated with each other to obtain effective solutions. The most important step in these kinds of analysis is a proper meshing process and some meshing examples are shown in Figure 2.10. Concerning to importance of the concept of analyzing methods, there is needed a brief explanation of them and the

remaining of this section will be continued by the explanation of these methods.

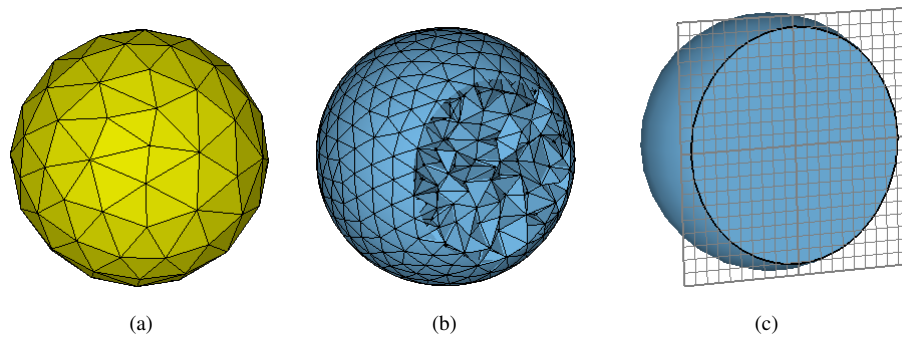


Figure 2.10. Three meshing examples obtained by CST-MWS (a) MoM surface mesh, (b) FEM tetrahedral mesh and (c) FDTD hexahedral mesh

In this regard, the integral equation solver of CST uses MoM which is one of the most widely used numerical methods for antenna engineering. The integral form of Maxwell's equations is reduced to matrix equations by applying the weighted residuals method (Sadiku, 2000; Rylander et al., 2012). Firstly, scattering surfaces of the structure are discretized by replacing them with equivalent surface currents. The matrices that represent each divided segment are derived and these matrices are iteratively filled with complex-valued inputs by utilizing iterative techniques. The set of linear equations is derived by applying boundary conditions to each element. After that, the current values on each segment are obtained by using the solution of these equations. The MoM method has many strong points that provide an effective solution for perfectly conductive surfaces, incorporate radiation conditions automatically and calculate important antenna parameters in a straightforward way directly or iteratively. This method applies only to homogeneous scatterers because this method requires volumetric mesh for non-homogeneous structures.

The most powerful solver of CST is the transient solver (time-domain) used finite integration technique (FIT) which is a relative of the FDTD method. FDTD is a preferred numerical analysis technique for structures operating at a wideband frequency range. It uses regular cubic or brick meshes and requires fine-mesh to model curved structures. The method is based on the solution of partial differential equations and approaches the differential operator in Maxwell curl equations on a grid in time and space gradually. Electric and magnetic fields are solved on the regular grid by proceeding in the time with the discretization of time and keeping the field components close to each other by using space offset (Sadiku, 2000; Rylander et al., 2012). To achieve accurate results mesh sizes must be much less than the smallest possible wavelength (which corresponds to the highest frequency of interest). This method uses a finite difference approach, which does

not set up and solve matrix equations. The method is widely preferred due to its ease in basic application and ensures an effective solution for non-homogeneous materials. But FDTD has problems such as the precise location of the boundaries and inflexible meshing. It cannot treat as efficient as MoM for perfect conductive scatterers.

CST uses the finite element method for its frequency domain solver. This technique was first proposed by Courant and began to use in the 1950s for structural mechanics and thermodynamics. Since then the FEM has been used for simulation and eigenvalue analysis of systems operating at microwave frequency range. It is a powerful numerical technique that offers efficient solutions for complex geometries and non-isotropic medium. This method solves partial differential Maxwell's equations approximately in frequency domain without any initial physical approximations being made (Sadiku, 2000; Jin, 2015). Some steps can be used to analyze any problem using the finite element method. In the first step, the geometry is divided into a large number of small elements that are connected to the nodes, which are the assembly point of sub-regions or elements. This subdivision process is called as meshing or discretizing and some typical examples of elements according to its dimension is shown in Figure 2.11. The discretization can be defined as the most important step because of the fact that it directly affects the calculation time and the accuracy of the numerical results (Jin, 2015).

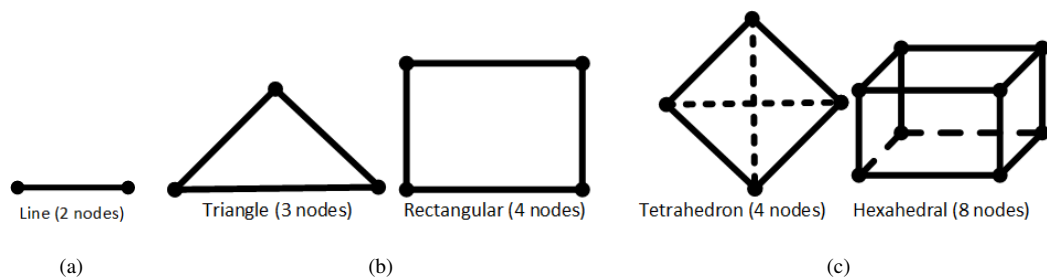


Figure 2.11. Finite elements (a) one-dimensional, (b) two-dimensional and (c) three-dimensional (Source: Sadiku, 2000)

The second step is the selection of an interpolation function to obtain the equation for a single element. Polynomials or trigonometric functions can be used as interpolation functions in accordance with the structure types. First (linear), second (second-order) or higher-order polynomials are often preferred for the finite element method because of providing convenience in the mathematical operation (Jin, 2015). Using higher grade polynomials increases accuracy, but it usually results in a more complex formulation and increase of computation time than using low-grade polynomials. After the determination of the polynomials, the solution for an element can be derived.

The third step is combining the equations obtained for all elements in the solution region. An approximate solution for the complete region can be derived by applying Ritz variational method or Galerkin's method to these collected equations.

The final step is to solve the system of equations for the entire solution region according to boundary conditions (Neumann or Dirichlet) applied to the structure.

In the thesis, in order to analyze the coupler structure we use both frequency and time domain solvers. The cavity is firstly analyzed with eigenvalue solver. Afterwards the coupler and its antenna is integrated to the pillbox cavity and the parameters of the complete structure is optimized for the critical coupling condition. The maximum power transfer from coupler to cavity is also verified by using frequency and time domain solvers.

CHAPTER 3

DESIGN AND FABRICATION OF THE PILLBOX CAVITY AND INPUT POWER COUPLER

The detailed information related to designs of the pillbox cavity and the power coupler and their results that are obtained by using CST-MWS will be described in the first section of this chapter. Afterward, results of cavity or coupler relevant parameters such as quality factors, resonance frequency, EM field distributions and S-parameters will be the next subject. The process of fabrication of the whole structure will also be summarized in this chapter.

3.1. Design of Input Power Coupler

Power couplers are a kind of transmission line designed to transfer power from an RF power source to a cavity. There are two types of couplers as waveguide and coaxial according to advantages or disadvantages. In this project, one has been decided to use coaxial coupler because of its small size and excellent coupling properties. In this context, a drum-like coupler which has been designed for 352.2 MHz at ESS Bilbao (as seen in Figure 3.1) is used as a basis for this study.

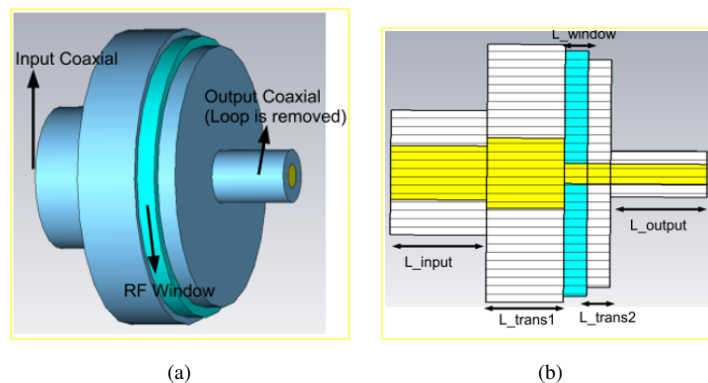


Figure 3.1. Drum-like coupler designed at ESS-Bilbao (a) full view, (b) cut view
(Source: Bermejo and Sordo, 2013)

Besides, it is worth noting that obtaining the maximum power transmission through a

coupler, losses should be decreased as much as possible at the operating frequency. In this regard, scattering parameters, which are briefly described in Section 2.5, has been used to determine losses due to reflection and mismatch. Aluminum and copper have been used as an outer conductor and an inner conductor, respectively, to reduce conductive losses for the coupler design obtained via the Frequency Solver of CST-MWS (as seen in Figure 3.2 and Figure 3.3). Also, couplers have to incorporate RF windows to separate the air side from the vacuum side. Hence, an RF window has been used in the middle of the coupler design and its material has been chosen as 99% alumina which has dielectric constant as $\epsilon_r = 9.5$ and dielectric loss tangent as $\delta = 6 \times 10^{-4}$ to obtain less dielectric losses.

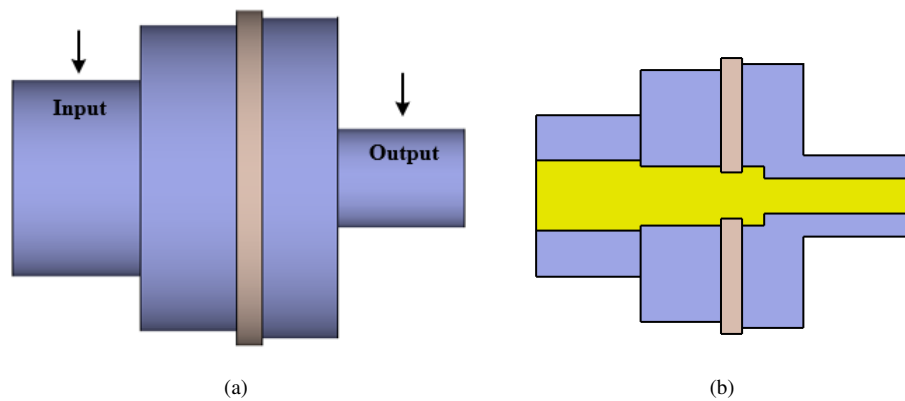


Figure 3.2. Input power coupler at 800 MHz (a) full view, (b) cut view

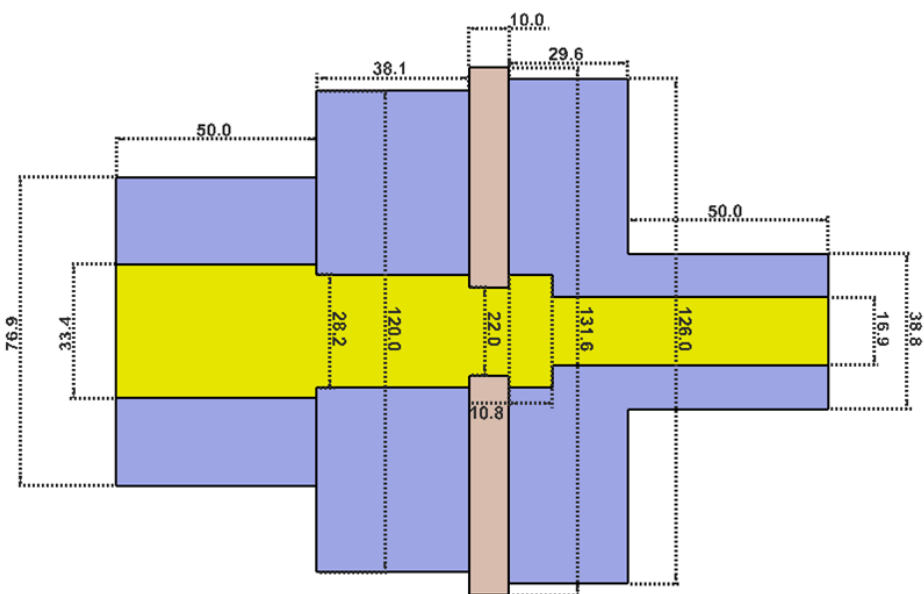


Figure 3.3. Dimensions (mm) of the input power coupler at 800 MHz

In Section 2.5, one has been expressed that the impedance matching is necessary to transfer the maximum power across the transmission line. Therefore the input and output port has been designed to match 50Ω and the other parameters have been changed by using parametric optimization to set the frequency as 800 MHz. The simulation result of the coupler design is shown in Figure 3.4. According to the S_{21} plot, 99.86% of input power is transmitted through power coupler by using the insertion loss (IL) equation.

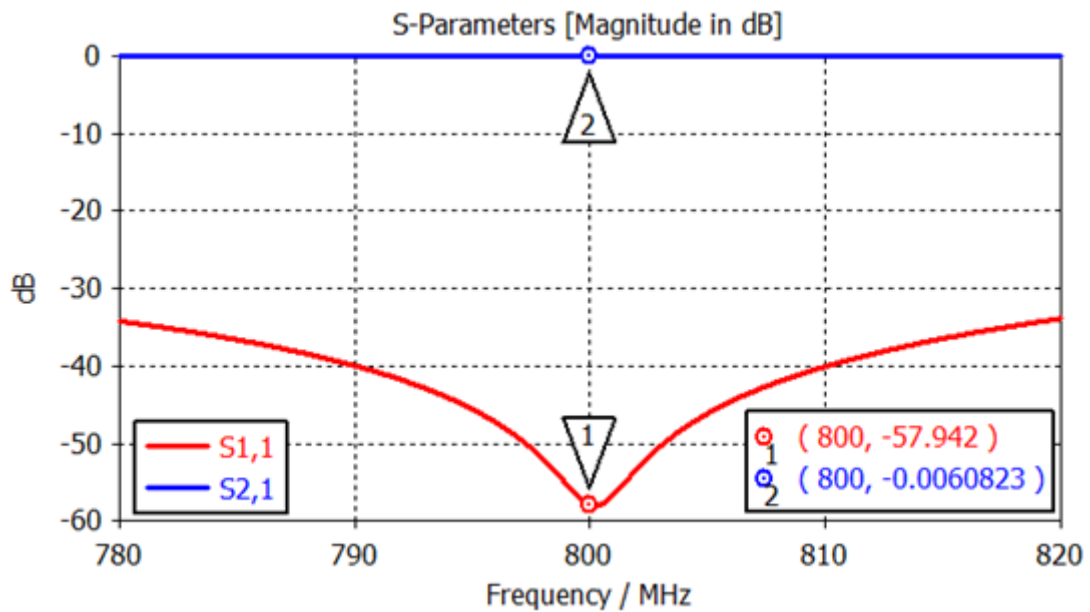


Figure 3.4. Scattering parameters of the input power coupler obtained via CST-MWS

3.2. Design of Pillbox Cavity

A cavity can be designed in different ways with respect to intended usage and producibility. In this study, the pillbox cavity has been used as a load to test the transmission line at 800 MHz. In this regard, there are two essential performance criteria. One of these parameters is resonance frequency, which determines the cavity dimensions. The other one is the quality factor which determines the loss of power in the cavity wall, as mentioned in Section 2.4. The electromagnetic calculations and 3-D designs have been made via the Eigenmode Solver of CST-MWS after the determination of material of cavity and tuner and medium inside the cavity. The 3-D shape and dimensions of the pillbox cavity are shown in Figure 3.5 and Figure 3.6, respectively.

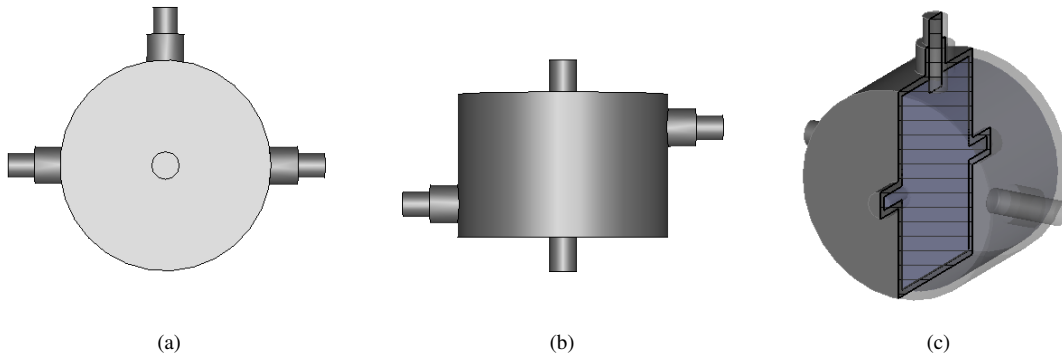


Figure 3.5. Pillbox cavity at 800 MHz (a) top view, (b) side view and (c) cut view

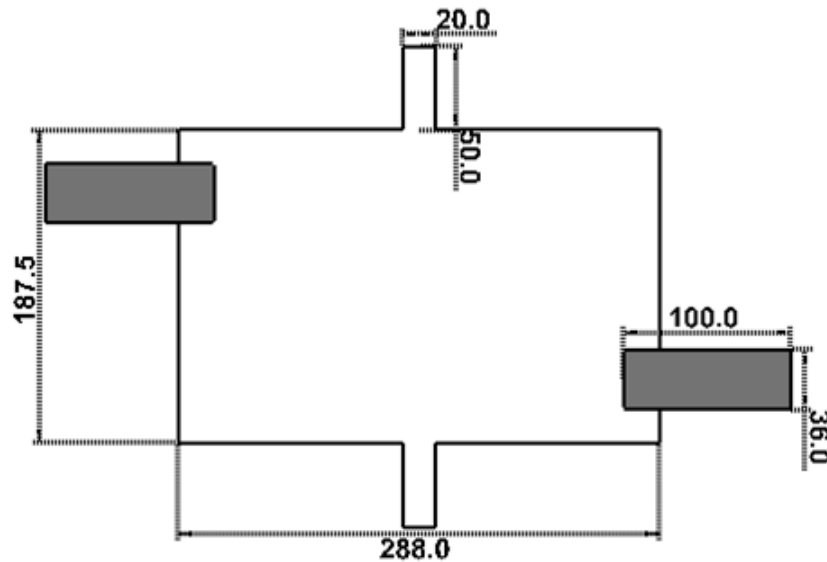


Figure 3.6. Dimensions (mm) of the pillbox cavity at 800 MHz

In this design, the most critical parameters are the cavity radius and length to determine the dominant mode and its frequency for resonating the microwave signal. The resonance frequency depends on the diameter of the cavity as proved in Section 2.3. However, the length of the cavity determines where the maximum value of the electric fields forms in the cavity. In order to achieve maximum fields in the middle of the cavity, the length is chosen as half of the wavelength at high frequencies and a quarter of the wavelength at low frequencies. To compensate production errors, three tuners have been added to the system like in Figure 3.1, additionally, the position and the diameter of these frequency arrangers have been specified by using the simulation program. The depth of the tuner has been adjusted as 20.36 mm from the surface of the cavity as seen in Figure 3.6. Consequently,

the electrical field distribution is seen as longitudinal and the magnetic field distribution is perpendicular to electric fields at 800.06 MHz concerning the desired mode TM_{010} as shown in Figure 3.7. In addition to this, the unloaded quality factor is computed as 26128 via the post-processing of CST, as seen in Figure 3.8.

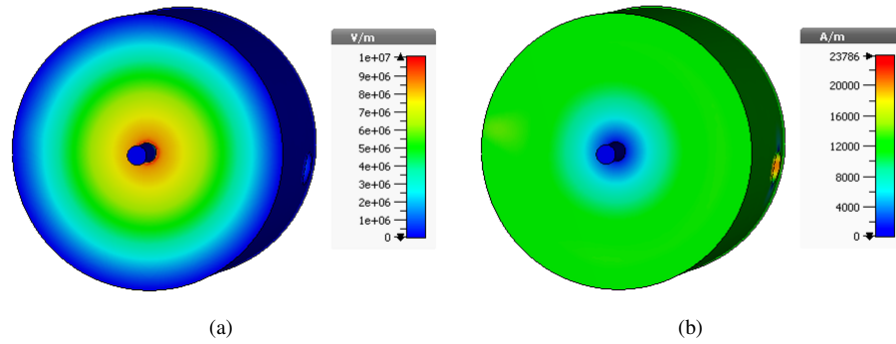


Figure 3.7. Absolute field distribution of pillbox cavity (a) electric field, (b) magnetic field

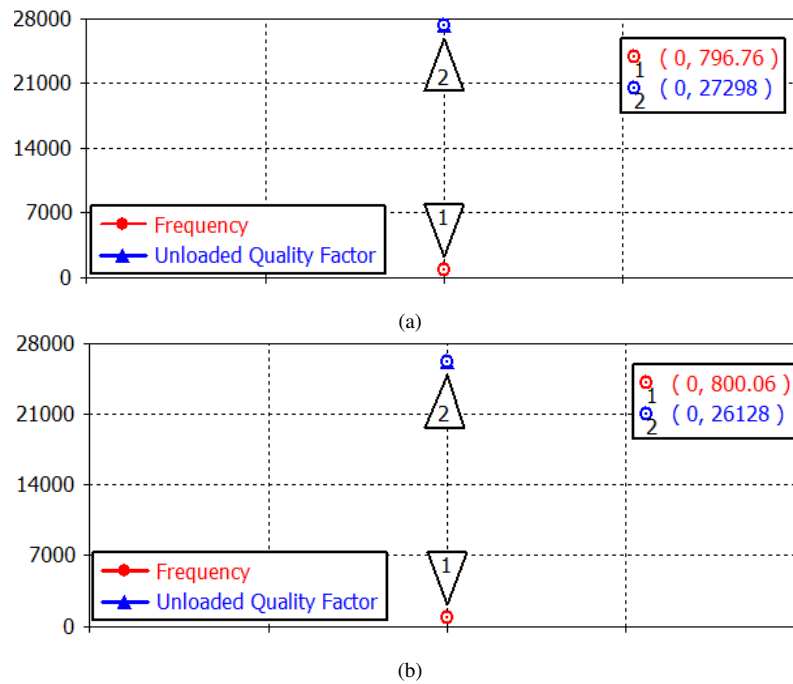


Figure 3.8. The resonance frequency and unloaded quality factor of pillbox cavity (a) without tuners, (b) with tuners

After the computation of the unloaded quality, the loaded quality factor and external quality factor have been calculated as 12921 and 25845, respectively by adding an antenna into the designed coupler to stimulate the fields inside the cavity. The most critical point of designing an antenna is to specify the dimensions according to the desired

results and producibility in associated with coupler dimensions. That's why the radius and inner lengths of the antenna have been chosen as 3.5 mm, 16.5 mm and 15.9 mm, respectively. The designed loop antenna attached to the coupler can be seen in Figure 3.9.

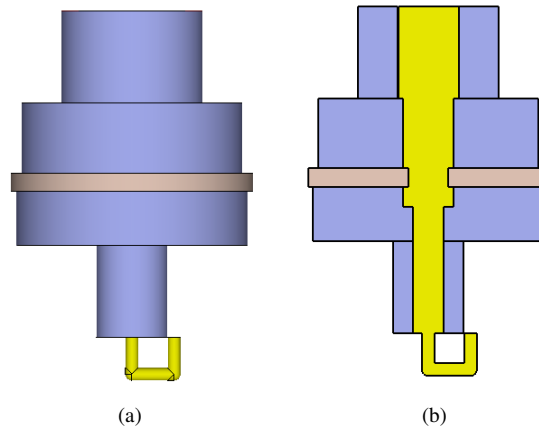


Figure 3.9. The loop antenna (a) full view, (b) cut view

To transmit RF power without any losses into a cavity, coupler and cavity system should operate together properly and this consistency is determined by beta (β), which is called a coupling coefficient. If the coupling coefficient equals to 1 ($\beta = \frac{Q_0}{Q_e} = 1$ where Q_0 is the unloaded quality factor and Q_e is the external quality factor), this situation is called as critical coupling. To obtain this parameter in the eigenmode solver, the cavity and the coupler are assembled as in Figure 3.10.

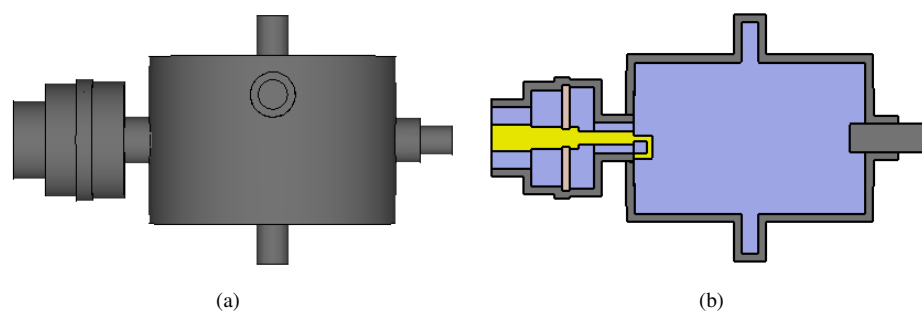


Figure 3.10. Coupler and cavity system (a) full view, (b) cut view

The coupling coefficient can be changed by rotating the antenna with respect to short circuit plain or modifying the antenna dimensions. The critical coupling (maximum power transmission) has been obtained in the eigenmode solver as seen in Figure 3.11 by rotating the antenna 104.55 degrees and by fixing the antenna dimensions and the depth

of three tuners. At the same condition, the electric and magnetic field distributions have been gained at 800.06 MHz as seen in Figure 3.12.

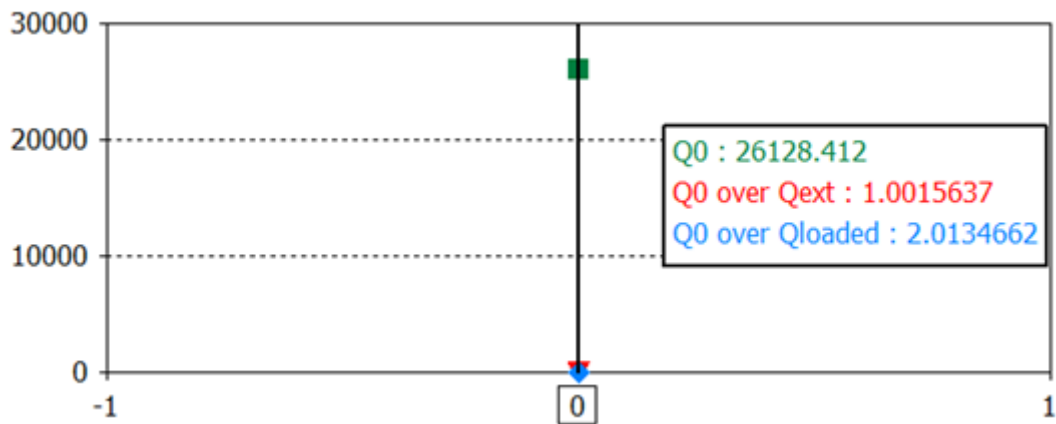


Figure 3.11. Critical coupling results of the coupler and cavity system via the Eigenmode Solver in CST-MWS

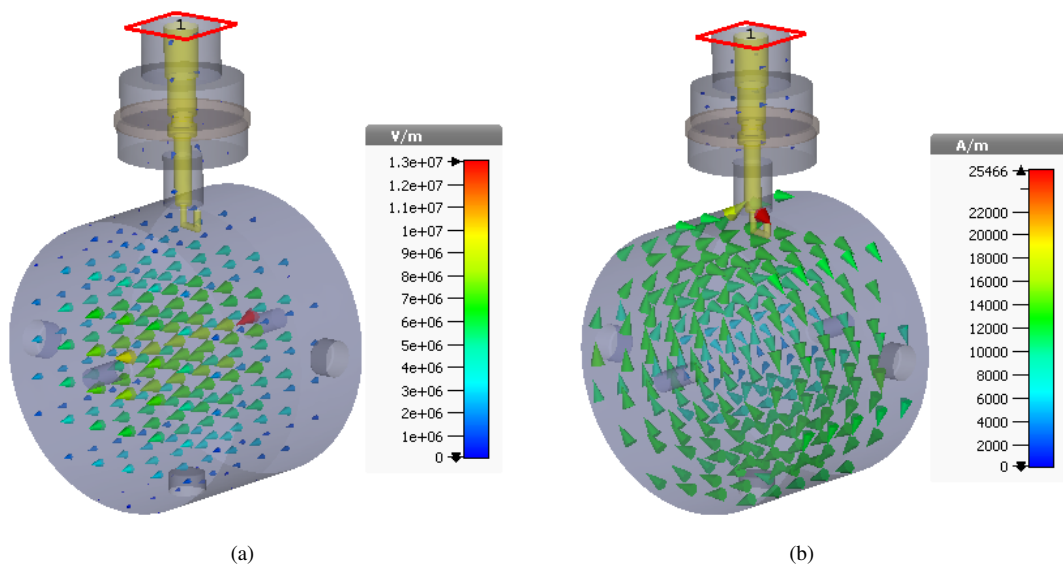


Figure 3.12. Field distribution of the coupler and cavity system (a) electric field, (b) magnetic field

In the critical coupling condition ($\beta = 1$), transfer of approximately entire power by coupler element is represented in Figure 3.11. At 800 MHz, this system transmits approximately the whole input power to the cavity as it is illustrated in Figure 3.13. According to these two results, the transmission of maximum power has been verified with both eigenmode solver and frequency solver.

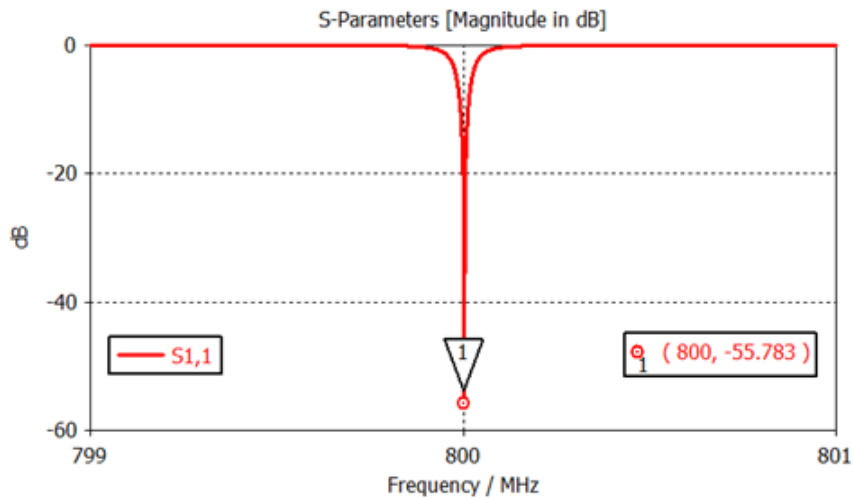


Figure 3.13. S_{11} of the coupler and cavity system obtained via the Frequency Solver in CST-MWS

3.3. Fabrication of Pillbox Cavity and Input Power Coupler

After the desired results of the cavity and the coupler were obtained by using 3D EM simulation, the Solidworks program (SOLIDWORKS, 2018) was used to make the whole structure ready for the production as shown in Figure 3.14.

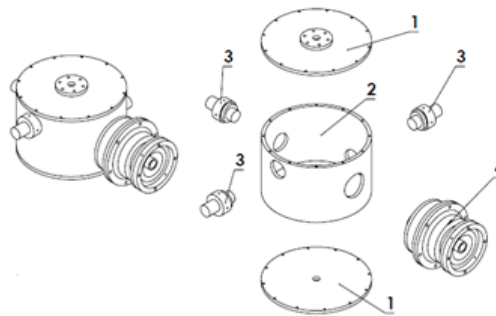


Figure 3.14. The parts of system mount

In order to facilitate both the production and the measurements to be taken, it was decided that the flange of the coupler on the side of the cavity and the transmission line would be movable flange as it is presented in Figure 3.15. Since the ratio of the power transferred to the cavity by the antenna that is connected to the coupler's internal conductor is determined by rotating the antenna, the bidirectional rotation provides structural convenience

for the measurements. Also, as shown in Figure 3.15, there is alumina at the part to which the input and output of the coupler are connected. In order to provide not damage to this part and ease of installation, the inner conductor of the coupler is connected to each other via screwing together and fixed to the output conductor via tight-fitting of the antenna.

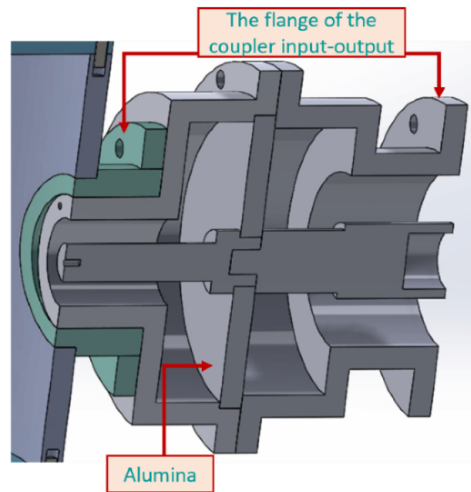


Figure 3.15. Coupler cut view

After the mechanical design, the production precision was determined as 100 microns in accordance with the 3D EM simulations, afterward, material supply and the production of the parts was started. It was decided to work with this company since a company called Plasbak in Beylikdüzü/İstanbul can produce the coupler with the desired precision. Aluminum 6013 was chosen because the cost and processing of material were more advantageous than other material types.



Figure 3.16. Photograph of materials before production

The material supply was taken according to the actual tolerance dimensions determined by the manufacturer, as shown in Figure 3.16. In this process, taking full cylinder because of the absence of the cylinder profile at the inner diameter and thickness of the cavity, which extended the production process. The material thickness was determined as 10 mm due to welding of the tuner flanges and the movable flanges of the coupler. In order to prevent surface distortions due to the heating of the material during the solder, the inner diameter of the cavity body was processed smaller and only small holes to center the flanges have been opened as shown in Figure 3.17. Also, the surface of the flanges was rounded by the CNC machine to fit them on the cavity surface.

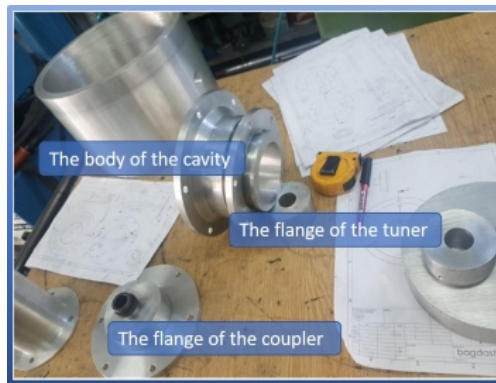


Figure 3.17. Photograph of parts before weld

After the welding process, all parts were processed one by one and the production was carried out successfully as shown in Figure 3.18.



Figure 3.18. The picture of the produced cavity and coupler

Then all the parts were brought to the Kandilli Detector, Accelerator and Instrumentation Laboratory (KAHVE) of Boğaziçi University and mounted as shown in Figure 3.3.



Figure 3.19. Photograph of dimensions of the whole structure

Moreover, the accuracy of production was measured to be on the order of tens of microns as can be seen from Table 3.1, which lists the measured and designed values of various dimensions of the components.

Table 3.1. The comparison list of designed and measured values of the parts.

Parameter	Designed Value (mm)	Measured Value (mm)
R	288	288.07
L	187.5	187.53

(cont. on next page)

Table 3.1 (cont.)

Parameter	Designed Value (mm)	Measured Value (mm)
<i>R1</i>	76.9	76.93
<i>L1</i>	50	49.9
<i>R2</i>	120	120.07
<i>L2</i>	38.1	38.13
<i>R3</i>	131.6	131.61
<i>L3</i>	10	10.05
<i>R4</i>	126	126.06
<i>L4</i>	29.6	29.61
<i>R5</i>	38.8	38.82
<i>L5</i>	50	50.07
<i>R6</i>	33.4	33.41
<i>L6</i>	50	50.11
<i>R7</i>	28.2	28.19
<i>L7</i>	38.1	38.09
<i>R8</i>	22	22.04
<i>L8</i>	10	10.09
<i>R9</i>	28.2	28.19
<i>L9</i>	10.8	10.81
<i>R10</i>	16.9	16.91
<i>L10</i>	68.8	68.8
<i>R11, R12, R13</i>	7	7.01
<i>L11, L13</i>	20	20.03
<i>L12</i>	22.9	22.8

CHAPTER 4

QUALITY FACTOR MEASUREMENTS OF PILLBOX CAVITY

A pillbox cavity and coupler, operating at 800 MHz have been designed, built and constructed. The two elements have been tested with varying methods. These measurements can be separated into two sections:

- measurement of quality factor and resonance frequency of the cavity by using various methods,
- determination of the performance of the system which is composed of the cavity and the coupler connecting with the transmission line at 100W provided from an RF power supply.

4.1. Measurements of Quality Factor

There are two measurement techniques based on reflection and transmission, which provide to measure the resonance frequency and the unloaded Q-factor of a cavity (Kajfez, 1999; Eberhardt, 2014). These methods are associated with measurements of the S-parameters that are obtained by using a vector network analyzer (VNA). As mentioned before in Section 2.5, when the cavity is connected to an input coupler the coupling coefficient β should be equal to 1 in order to ensure that most of the power is transferred to the cavity. In contrast to $\beta = 1$, at the low beta indicates that more power is lost in the cavity and at high beta, power is lost in the external connected elements, like coupler and transmission line. Also, β is related to loaded, external and unloaded Q-factors and this can be expressed as:

$$\frac{1}{Q_\ell} = \frac{1}{Q_0} + \frac{1}{Q_e} \quad \text{and} \quad \beta = \frac{Q_0}{Q_e} \quad (4.1)$$

By combining these two equations, the loaded Q-factor (Q_ℓ) formula can be turned into:

$$Q_\ell = \frac{Q_0}{1 + \beta} \quad (4.2)$$

The unloaded Q-factor (Q_0) cannot be calculated directly by using measurement techniques, but the approximate value of Q_0 can be obtained using Equation 4.2. Here, it is necessary for the coupling coefficient to be as close to zero as possible to get an accurate measurement that provides Q_ℓ is approximately equal to Q_0 . Concerning that, the value of Q_ℓ can be calculated with -3dB rule which can be acquired from reflection or transmission graph of S-parameters as:

$$Q_\ell = \frac{f_0}{f_{-3\text{dB}}^+ - f_{-3\text{dB}}^-} \quad (4.3)$$

where f_0 is the resonance frequency that is expressed as the maximum or minimum point of S-parameter graphs according to frequency. Also, $f_{-3\text{dB}}^+$ and $f_{-3\text{dB}}^-$ are frequencies corresponding to -3dB drop of these points. In this regard, reflection and transmission measurement methods were used to determine unloaded Q-factor and resonance frequency of the cavity by using -3dB rule in the sections below. For each measurement of S-parameters, the frequency range of VNA was adjusted between 799.5 MHz and 800.5 MHz with 4001 sweep points and IF bandwidth of 10 kHz was chosen. Also, minimum reflection and maximum transmission values were taken at operating frequency by adjusting tuners according to the highest efficiency places and results are plotted via software (MATLAB, 2019).

4.1.1. Reflection-Type Measurement at Critical Coupling

One connection port is sufficient for the reflection measurement (Kajfez, 1999). This port on the cavity is connected to the port of VNA. After the reflection coefficient (S_{11}) is adjusted to a minimum at resonance frequency to obtain the critical coupling condition, -3dB points are found. Then these obtained values are calculated by inserting into Equation 4.3 to get the unloaded Q-factor of the system, but this is not so easy. Concerning this, to determine whether the system provides the critical coupling condition, the Smith Chart can be used, as shown in Figure 4.1.1. When the real and imaginary parts of the impedance are equal to each other as; $Re\{Z\} = Im\{Z\}$ with the angle $\phi = \pm 45^\circ$ and also the magnitude of the impedance is equal to $|Z| = 0.707R$ where R is the radius of circle, one can say that the system is critically coupled (Caspers, 2012). The matching condition is also determined by looking to the occurring circle on the Smith Chart. If the radius of the circle is equal to one ($R = 1$), the coupling coefficient becomes one according to equation ($\beta = \frac{1}{\frac{2}{R}-1}$ (Kajfez, 1999)). This matching condition is called “critical coupling”. If the radius is less (more) than one, the condition is called weak

(over) coupling. The condition for transmitting the maximum power can be calculated by using the relation of $Q_0 = 2Q_\ell$.

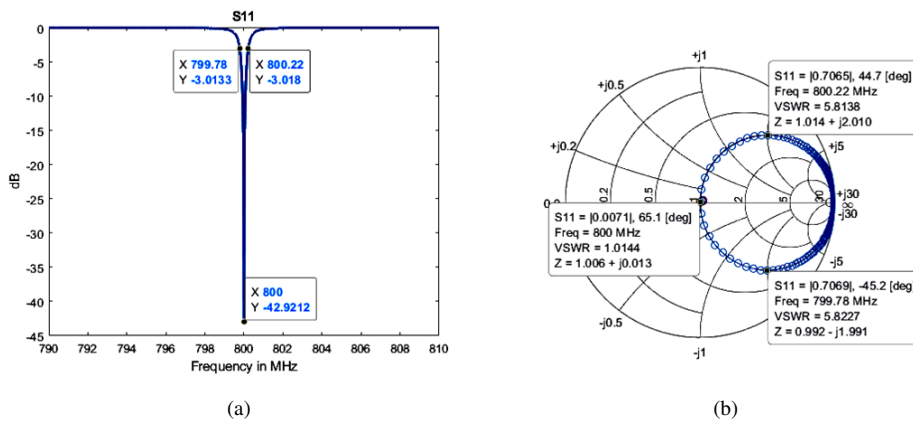


Figure 4.1. Representation of quality factor measurements from (a) S_{11} , (b) Smith chart

The experimental setup for the reflection type measurement was performed, as shown in Figure 4.2. After commissioning the whole components of the cavity with the coupler, N-type connector (whose inner and outer radius were 33.40 mm and 76.90 mm, respectively) was used at the input port of the coupler to get measurements from VNA.



Figure 4.2. Reflection type measurement setup

For the measurements, three tuners that were implemented to the cavity for frequency shift and the fixed antenna on the power coupler should have been optimized according

to the operating frequency. The optimization of tuners was done by changing the locations of them and the optimization of the coupler was done by rotating. As a result of these arrangements, the reflection type measurement results have obtained, as shown in Figure 4.3. The loaded Q-factor was determined by using -3dB points on the plot then $Q_0 = 17260$ was calculated by using the relation $Q_0 = 2Q_\ell$.

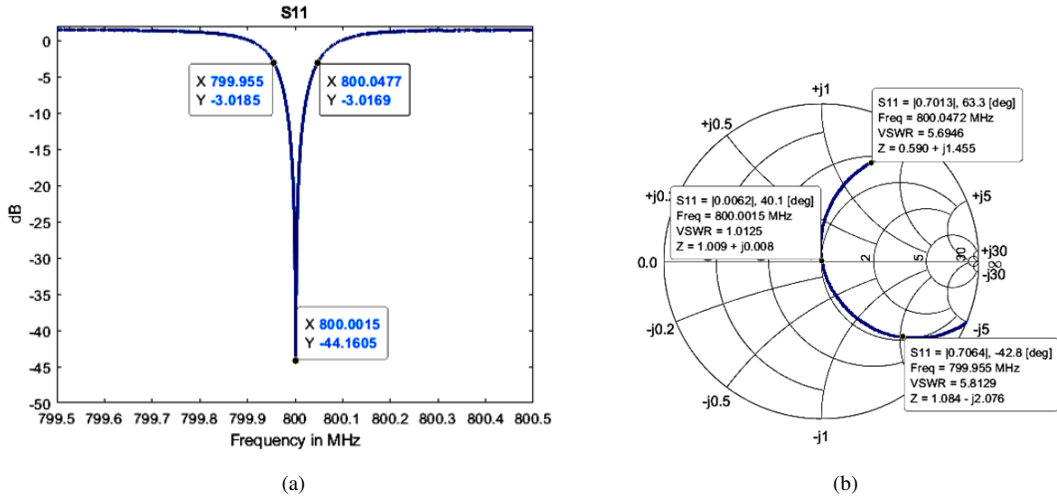


Figure 4.3. The reflection type measurement results (a) -3dB points of S_{11} , (b) its Smith chart representation.

4.1.2. Transmission Type Measurement

Transmission type measurement is realized by using two connection ports. These ports on the cavity are connected to the ports on VNA. The loaded Q-factor of the system is calculated in the below Equation 4.4 by inserting -3dB drop points from the graph of the transmission coefficient S_{21} (Caspers and Kowina, 2014; Bray and Roy, 2004).

$$Q_\ell = \frac{f_0}{f_{-3dB}^+ - f_{-3dB}^-} \quad (4.4)$$

The input and the output ports, which are used for transmission measurement, have different coupling coefficient values as β_1 and β_2 . Accordingly, the coupling coefficient for the ports can be computed by the following formula as (Kajfez, 1999):

$$S_{21}(f_0) = \left(\frac{2\sqrt{\beta_1\beta_2}}{1 + \beta_1 + \beta_2} \right) \quad (4.5)$$

For the critical coupling, the individual coupling coefficients of each port have to be equal to each other. According to this equality, the formula for the computation of coupling

coefficients can be modified and the relation can be obtained as $\beta = 2\beta_1 = \frac{S_{21}(f_0)}{1-S_{21}(f_0)}$. By combining this formula with Equation 4.2, the unloaded quality factor formula is turned into version as below:

$$Q_0 = \left(\frac{Q_\ell}{1 - S_{21}(f_0)} \right) \quad (4.6)$$

Here, the unit of $S_{21}(f_0)$ is a linear value that is found by writing the dB value f_0 instead of α in this formula $S_{21}(f_0) = 10^{\frac{\alpha}{20}}$. For realistic measurements of the quality factor, the dimensions of the measurement points, as well as the antennas, are two critical factors in the efficiency of the determination of the quality factor (Kajfez, 1999).

In this study, since the excitation of the cavity is done with a single port, the second ports are selected from the different points on the cavity. As seen in Figure 4.4, these points are labeled as hole, coupler flange, beam pipes and tuner1,2,3 flanges to understand the experimental setups. Critical coupling is the significant condition for the measurements however for the following measurements weak coupling was chosen because of the unequal size of two antennas. Due to obtaining weak coupling, zero transmission ($S_{21}(f_0) \rightarrow 0$) was ensured in the measurement and the equality conditions of the loaded Q-factor and unloaded Q-factor ($Q_\ell \cong Q_0$).

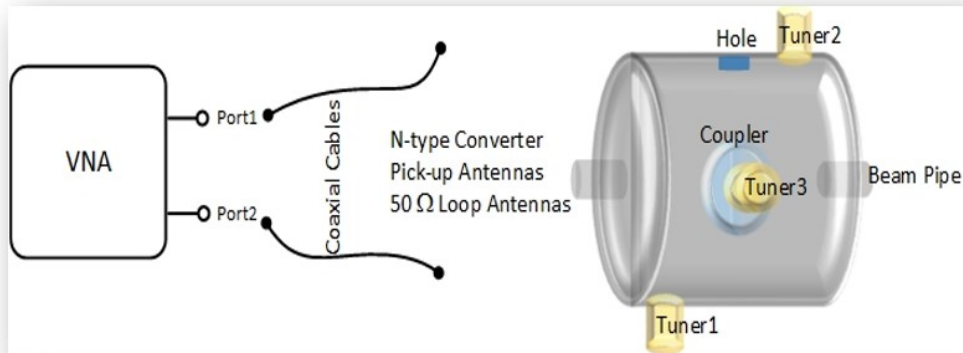


Figure 4.4. General scheme of transmission type measurement

The two antennas mentioned in the transmission method were also designed and build for this specific measurement as shown in Figure 4.5 and Figure 4.6. The purpose of these special antennas is to disturb as small as possible area volume inside the cavity and to possess realistic measurement results about the electromagnetic fields inside the cavity. The process of building 50Ω loop antennas has been started by welding to two N-type connectors via a short copper wire (as shown in Figure 4.6). In order to get 50Ω impedance at the operating frequency range, appropriate L and C values were welded

between the two connectors. The impedance of antenna depends on the thickness of wire and the radius of loop and these values have been optimized by using the impedance matching method in the Smith chart. Eventually, $120\mu H$ inductance was used for the antenna1 and $80\mu H$ inductance with $75pF$ capacitor was utilized for the antenna2.



Figure 4.5. The photograph of pick-up antennas

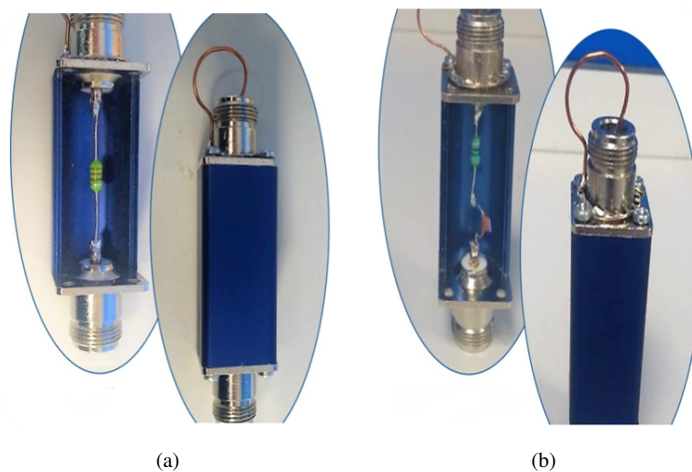


Figure 4.6. Photographs of the designed 50Ω loop antennas (a) cut and full view of antenna1, (b) cut and full view of antenna2

After constructed the intended loop antennas, the results of impedance measurements were obtained as shown in Figures 4.7 and 4.8. Several experimental setups were performed and explained in the following sections according to the measured locations from the flange of the coupler, flanges of the three tuners (1,2,3) from the hole on the cylindrical

wall of the cavity and the beam pipes as shown in Figure 4.4.

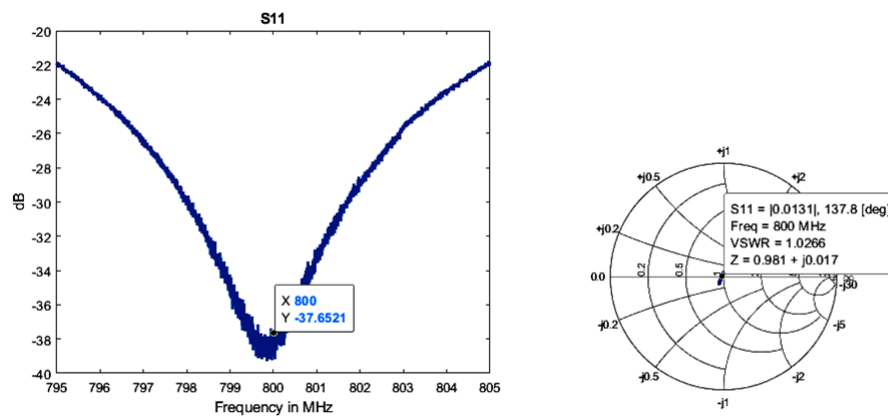


Figure 4.7. Results of reflection coefficient and impedance plot for 50Ω loop antenna1 outside of the cavity

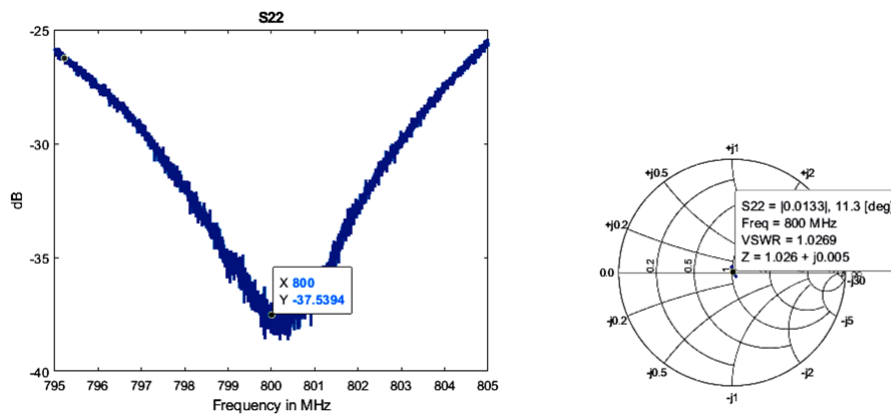


Figure 4.8. Results of reflection coefficient and impedance plot for 50Ω loop antenna2 outside of the cavity

4.1.2.1. Experimental Setup 1

Here, the quality factor was measured by inserting the pick-up antennas shown in Figure 4.9 through the beam pipes. The aim is to measure the natural frequency of the cavity and the loaded quality factor. Therefore, all tuners were taken out and all hollow flanges were covered with metal tape. The resonance frequency of the cavity can be calculated by using the plot of the transmission coefficient S_{21} . The frequency that corresponds to the maximum peak value in the chart is called resonance frequency as

seen in Figure 4.10. Hence, the resonance frequency of the cavity without tuners was measured as 794.59 MHz. In order to measure unloaded quality factor, Equation 4.4 can be used with the minimum transmission method that subjects to $Q_\ell \cong Q_0$. -3dB points of the S_{21} graph are shown in Figure 4.10. By inserting these values into Equation 4.4, the value of the unloaded quality factor was obtained approximately 19865 for this experimental setup. Besides this, the calculation process of the unloaded quality factor will be the same manner for the next experimental setups.



Figure 4.9. Experimental setup 1 with pick-up antennas

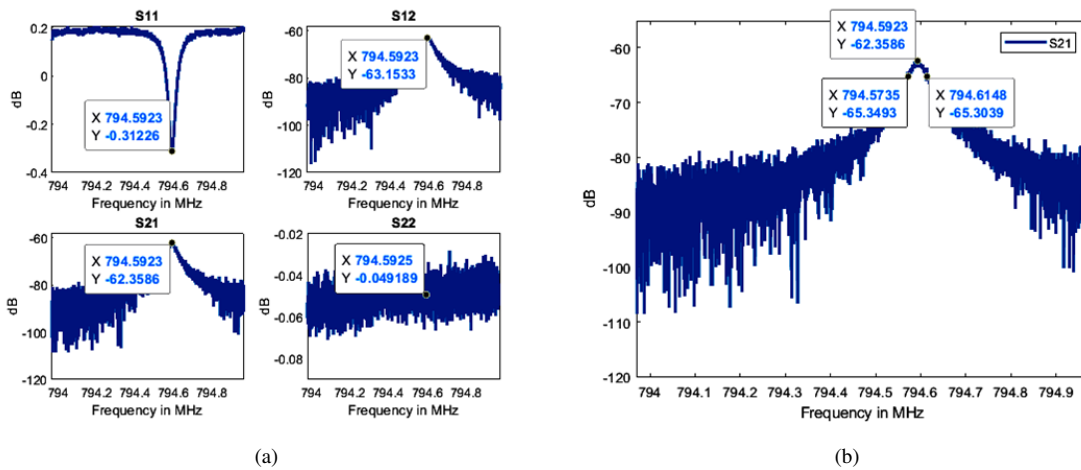


Figure 4.10. (a) S-parameters results (b) -3dB points of S_{21} for experimental setup 1

4.1.2.2. Experimental Setup 2

This experimental setup was realized by measuring through the flange of the coupler and tuner3 as shown in Figure 4.11. Tuner1 and tuner2 were taken off and their flanges

were covered by metal tape. The weak coupling condition was obtained by the rotation of the antennas and the unloaded quality factor and the resonance frequency were measured as 16492 and 794.897 MHz, respectively.



Figure 4.11. Experimental setup 2 with 50Ω loop antennas.

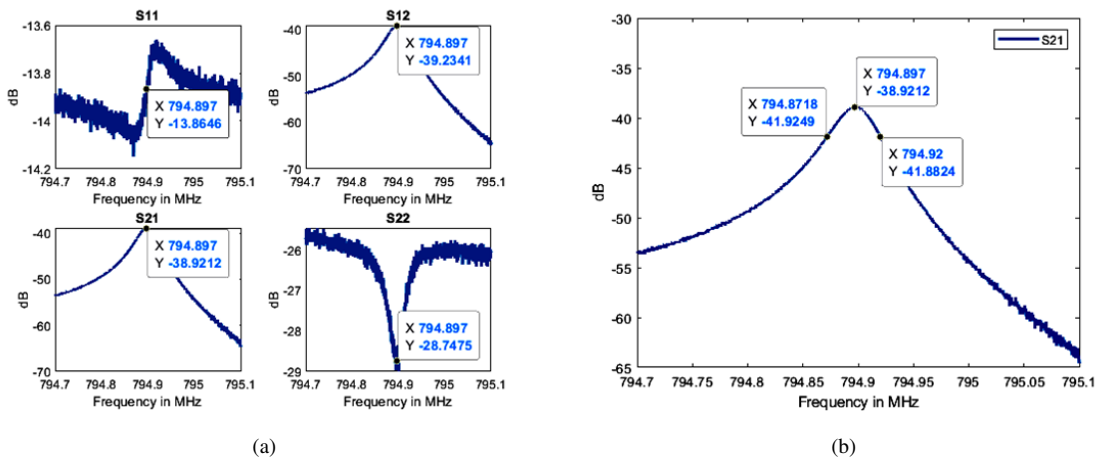


Figure 4.12. (a) S-parameters results (b) -3dB points of S_{21} for experimental setup 2

4.1.2.3. Experimental Setup 3

This measurement was performed by using the input power coupler and one of the pick-up antenna, which was inserted into the hole with equipment on the cylindrical wall of the cavity (as shown in Figure 4.13). The quality factor was computed as 14760

at 800 MHz by optimizing both the coupler antenna and the tuners to obtain minimum transmission.

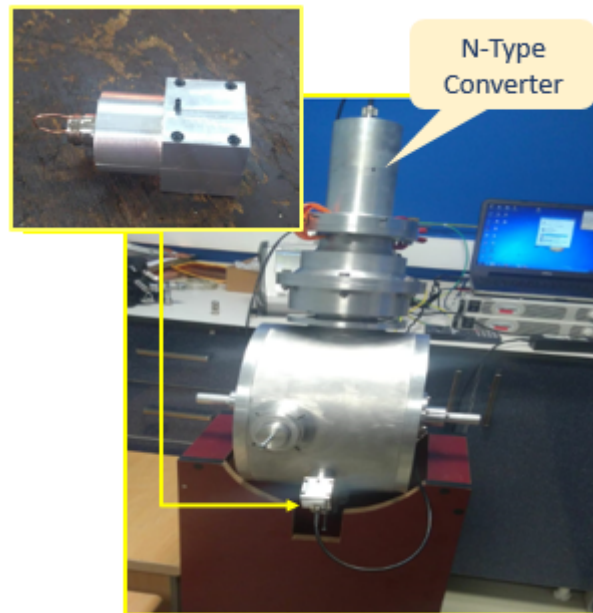


Figure 4.13. Loaded quality factor measurement setup 3 with pick-up antenna

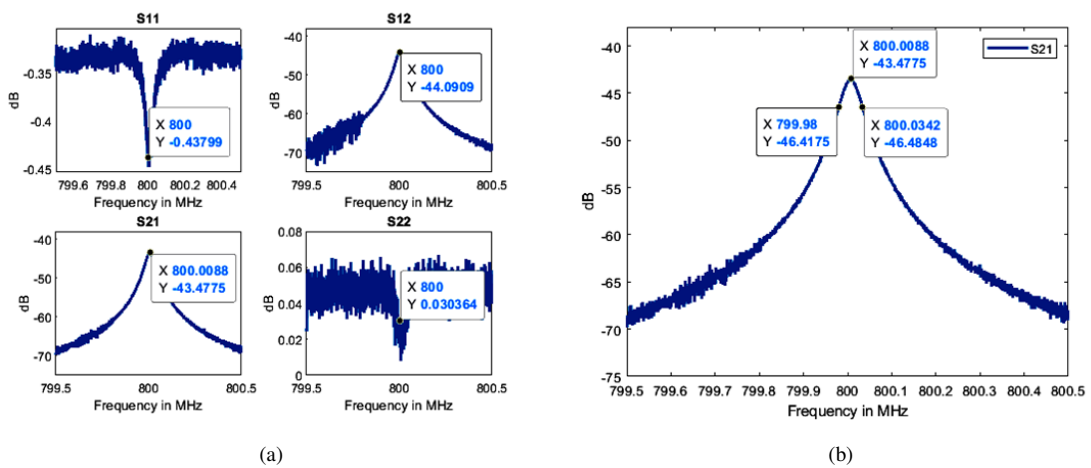


Figure 4.14. (a) S-parameters results (b) -3dB points of S_{21} for experimental setup 3

4.1.2.4. Experimental Setup 4

As seen in Figure 4.15, the fourth measurement was done by using across holes, which were the couplers flange and the hole of tuner3. The remaining holes of the other

tuners were positioned in the full side to approach 800MHz. The quality factor was measured as 14867 according to Figure 4.16.

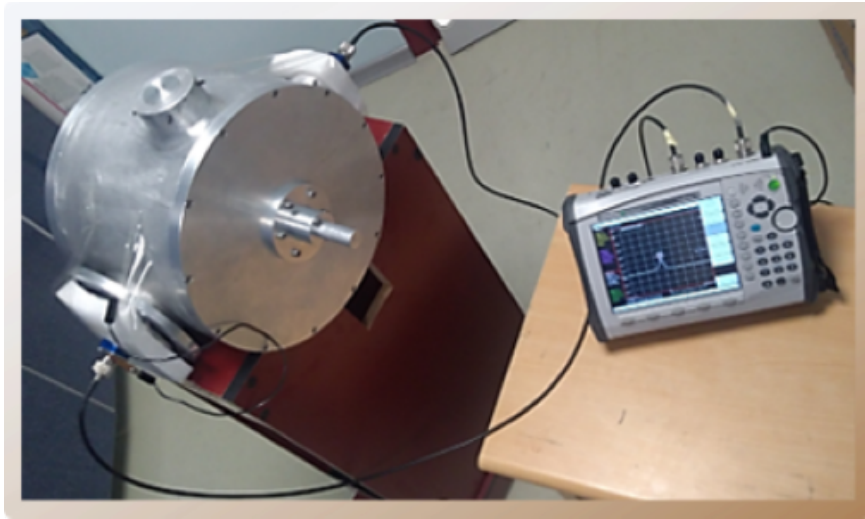


Figure 4.15. Loaded quality factor measurement setup 4 with 50Ω loop antennas

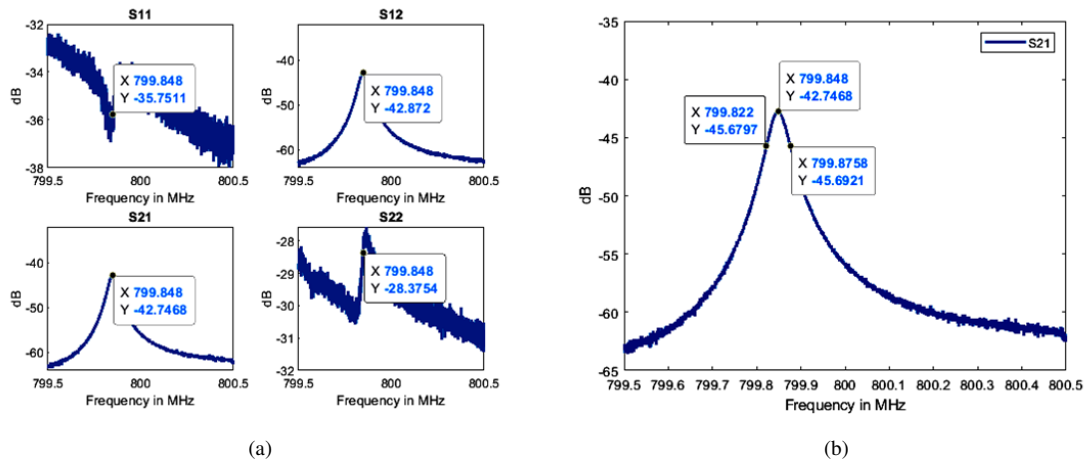


Figure 4.16. (a) S-parameters results (b) -3dB points of S_{21} for experimental setup 4

4.1.2.5. Experimental Setup 5

The measurement in this experiment was done by using beam pipes holes. As shown in Figure 4.17, the entrance of the coupler flange was covered by metal tapes and the tuners were positioned according to the operating frequency and as well as the placed

antenna was rotated to get the weak-coupling condition. The unloaded quality factor was measured as 15038 by using -3dB rule at transmission plot as shown in Figure 4.18.



Figure 4.17. Loaded quality factor measurement setup 5 with pick-up antennas

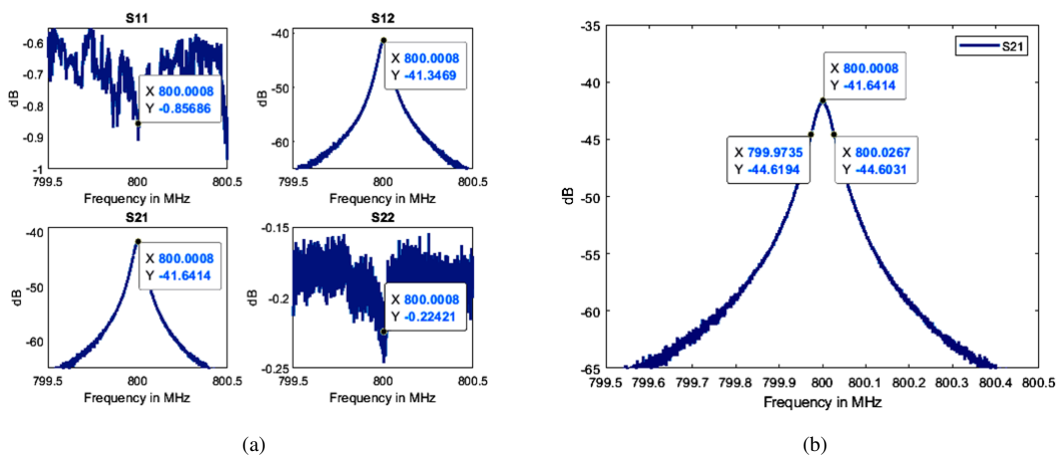


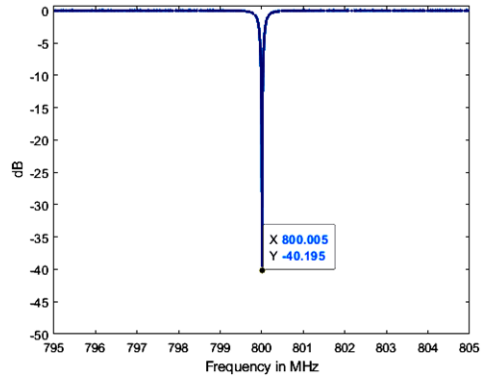
Figure 4.18. (a) S-parameters results (b) -3dB points of S_{21} for experimental setup 5

4.2. Power Measurement of the System

Measurements in this section were performed by installation the cavity and the transmission line as well as applying 100W power. As a first step, the cavity and coupler system were adjusted to have minimum the S_{11} at 800 MHz by rotating the coupler antenna and adjusting the tuner positions for ensuring the maximum power transmission condition (as shown in Figure 4.19).



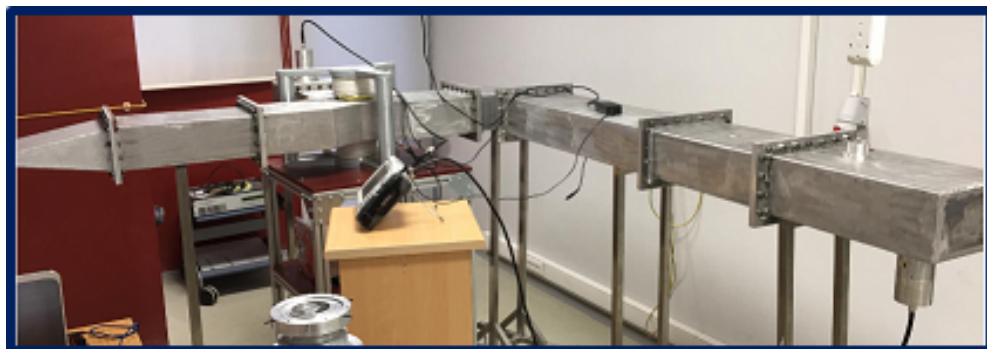
(a)



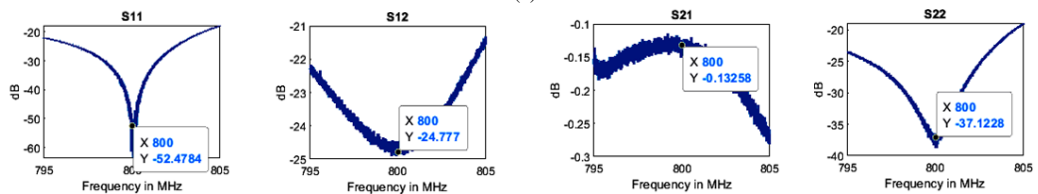
(b)

Figure 4.19. (a) Measurement test stand of the cavity (b) result of the S_{11} parameter of the cavity and coupler system

After the first step, the transmission line (as shown in Figure 4.20) was measured by using the VNA and the system was fixed after maximizing the transmission coefficient by adjusting the position of tuners. After that, cavity and coupler system was connected to the transmission line as shown in Figure 4.21.



(a)



(b)

Figure 4.20. (a) Measurement test stand of the transmission line (b) the result of the S-parameters of the transmission line



Figure 4.21. Power measurement test stand of the whole system.

Before the high-power measurements, the 40dB attenuator used to protect the measurement devices as shown in Figure 4.22.a. Firstly, the determination of the direction of the attenuator was done by measuring S-parameters. As a result of measurements, one was determined that the attenuator can be used in two directions. After that, the RF power supply and the attenuator were connected to each other (as shown in Figure 4.22) to determine how much power is obtained from the RF power supply by using the spectrum analyzer. The measurement results are listed as shown in Table 4.1.



(a)



(b)

Figure 4.22. (a) Attenuator test setup via VNA (b) power determination of RF power supply via spectrum analyzer

Table 4.1. The amount of power supplied from the RF power supply to the system.

Attenuator=-40dB → transmit 0.01% of power			
RF Power Supply (W%)	Spectrum Analyzer (dBm)	dBm to mW	RF Power (mW)
0%	-51.5	7.110^{-6}	0.071
5%	-49.5	1.110^{-5}	0.11
10%	-47.2	1.910^{-5}	0.19
15%	-45.1	3.110^{-5}	0.31
20%	-43.1	4.8910^{-5}	0.48
25%	-41.4	7.210^{-5}	0.72
30%	-36.7	2.110^{-4}	2.1
35%	-25.7	2.710^{-3}	27
40%	-16.8	2.110^{-2}	210
45%	-10.9	8.110^{-2}	810
50%	-5.9	0.26	2600
55%	-2.2	0.6	6000
60%	0.9	1.23	12300
65%	3.1	2.04	20400
70%	5.2	3.3	33000
75%	6.8	4.78	47800
80%	8.1	6.46	64600
85%	9	7.94	79400
90%	9.7	9.33	93300
95%	10.1	10.2	102000
100%	10.5	11.2	112000

Furthermore, in the same measurement setup in Figure 4.21, the parameter S_{21} was set as minimum as possible by changing the depth of the insertion of the 50Ω pick-up antenna into the cavity. During the experiment, the S_{21} parameter values were measured against the distance of the antenna entering by using VNA. Afterward, the power values were measured via the spectrum analyzer by giving high power gradually without changing the position of the antenna. The measurement results were obtained by following the procedure below.

- The transmission parameter S_{21} was set to a minimum via measuring VNA and its measured value was obtained, as shown in Figure 4.23. Afterward, the position of the cavity, transmission line tuners and the antenna were fixed.
- 40dB attenuator was connected to antenna output to reduce power and then the attenuator other port was connected to the spectrum analyzer with a coaxial cable to

measure power. Finally, while the power of the RF power supply was gradually given to the system the power which was transported to the cavity by the transmission line was measured by the spectrum analyzer and measured results are listed in the following table. All in all, the transmission line was fed up via the RF power supply reach up to a maximum 112 W and 0.021% of the power has been got lost according to Table 4.2.

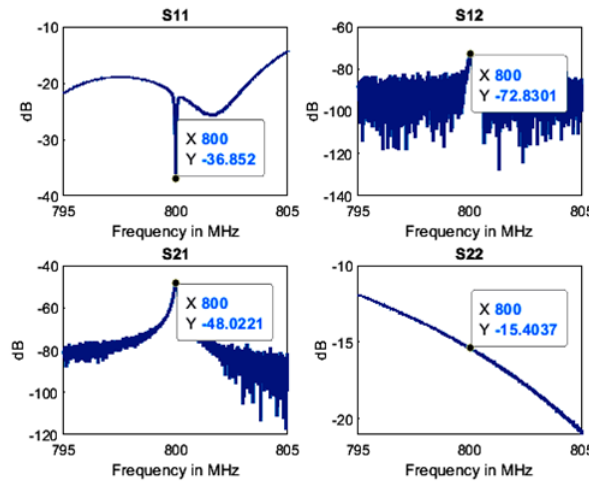


Figure 4.23. S-parameter results of the power measurement test setup of the whole system

Table 4.2. The results of whole system power measurement.

Attenuator = $-40dB$ \rightarrow transmit 0.01% of power $S_{21} = -48.02dB$ \rightarrow transmit 0.0016% of power $S_{11} = -36.85dB$ \rightarrow reflect 0.0207% of power					
RF Power (mW)	Spectrum Analyzer (dBm)	dBm to mW	Pick-up Power (mW)	Reflected Power (mW)	Stored Power into Cavity (mW)
0.071	-81	7.910^{-9}	7.910^{-5}	1.510^{-5}	0.0709
0.11	-80	1.10^{-8}	1.110^{-4}	2.310^{-5}	0.1098
0.19	-79	1.310^{-8}	1.310^{-4}	3.910^{-5}	0.1898
0.31	-79	1.310^{-8}	1.310^{-4}	6.410^{-5}	0.3098
0.48	-78	1.610^{-8}	1.610^{-4}	9.910^{-5}	0.4797

(cont. on next page)

Table 4.2 (cont.)

Attenuator=-40dB → transmit 0.01% of power $S_{21} = -48.02dB \rightarrow$ transmit 0.0016% of power $S_{11} = -36.85dB \rightarrow$ reflect 0.0207% of power					
RF Power (mW)	Spectrum Analyzer (dBm)	dBm to mW	Pick-up Power (mW)	Reflected Power (mW)	Stored Power into Cavity(mW)
0.72	-76	2.510^{-8}	2.510^{-4}	1.510^{-4}	0.7196
2.1	-75	3.210^{-8}	3.210^{-4}	4.310^{-4}	2.099
27	-72.5	5.610^{-8}	5.610^{-4}	5.610^{-3}	26.99
210	-658	3.210^{-7}	3.210^{-3}	0.04	209.956
810	-59.79	1.110^{-6}	0.011	0.17	809.819
2600	-53.1	4.910^{-6}	0.049	0.54	2599.411
6000	-50.4	9.110^{-6}	0.091	1.2	5998.709
12300	-47.9	1.610^{-5}	0.16	2.5	12297.34
20400	-45.4	2.910^{-5}	0.29	4.2	20395.51
33000	-43.6	4.410^{-5}	0.44	6.8	32992.76
47800	-42	6.310^{-5}	0.63	9.9	47789.47
64600	-40.9	8.110^{-5}	0.81	13.3	64585.89
79400	-40.1	9.810^{-5}	0.98	16.4	79382.62
93300	-38.5	1.410^{-4}	1.4	19.3	93279.3
102000	-38	1.5810^{-4}	1.58	21.1	101977.32
112000	-37.6	1.710^{-4}	1.7	23.2	111975.1

CHAPTER 5

CONCLUSION

This thesis covers topics related to the design, simulation and production of the pillbox cavity and the power coupler, which are two crucial sub-systems of the RF circulator and transmission line project. Firstly, 3-D design and electromagnetic calculations of the cavity have been obtained by using the Eigenmode Solver in the CST-MWS. The dimensions of the cavity to oscillate TM_{010} fundamental mode at 800 MHz have been determined with the help of this solver. Then, three tuners have been added to the cavity to adjust for and overcome shifts in the resonance frequency, thus taking into account possible faults in production. The resonance frequency and the unloaded quality factor of the cavity have been computed as shown in Table 5.1.

Table 5.1. The resonance frequency and the unloaded quality factor of pillbox cavity computed for $\sigma = 3.5610^7 S/m$ via the Eigenmode Solver in CST-MWS

	f_{res} (MHz)	Q_0
Pillbox cavity with tuners	800.06	26128
Pillbox cavity without tuners	796.76	27298

Afterward, the power coupler, which enables to transfer of power into the cavity, has been designed by using the Frequency Solver of CST-MWS. In order to transmit the power without loss, the reflection S-parameters should be minimum and the transmission S-parameters should be maximum at 800 MHz. The simulation results of the coupler are listed in Table 5.2, which shows that 99.86% of input power is transmitted through the power coupler according to the transmission coefficient (S_{21}).

Table 5.2. The S-parameter values of the input power coupler obtained via the Frequency Solver in CST-MWS

	S_{11} (dB)	S_{21} (dB)
Input Power Coupler	-57.942	-0.0061

In the last part of the design process, the loop antenna has been designed to stimulate

fields within the cavity and then the whole system is combined and the loaded and the external quality factors of the cavity have been calculated as seen in Table 5.3.

Table 5.3. The values of the resonance frequency and the quality factors of the cavity and coupler system obtained via the Eigenmode Solver in CST-MWS

	Q_0	Q_{ext}	Q_t	f_{res} (MHz)
Cavity and Coupler System	26128	25845	12921	800.06

In order to transfer of approximately entire power by the coupler element, the coupling coefficient $\beta = \frac{Q_0}{Q_{ext}}$ should be close to 1. According to Table 5.3 this condition is satisfied successfully. Also, the S-parameter results of the whole system have also been obtained as given in Table 5.4. At 800 MHz, this system transmits approximately the whole input power to the cavity related to Table 5.4.

Table 5.4. The S-parameters of the cavity and coupler system obtained via the Frequency Solver in CST-MWS

	S_{11} (dB)	f_{res} (dB)
Cavity and Coupler System	-55.783	800

Thus having achieved simulation results, Solidworks is used to make the structure ready for production. During this step, all the mechanical components have been considered in detail in terms of both ease of manufacture and facilitating the measurements to be taken.

After the successful completion of production phase and the assembling of the whole parts, measurements have been performed in two parts; the first is to measure the quality factor of the cavity with different methods, the second is to connect the cavity and the power coupler to the transmission line and to test the whole system up to 100Watts with an RF power source. In order to determine unloaded quality factor and resonance frequency, transmission and reflection S-parameters are measured from the different points on the cavity. These points are seen in Figure 4.4 and they indicate the Port1 and Port2 locations in Table 5.5. For quality factor measurements, N-type converter, pick-up antennas and 50-ohm loop antennas are used as Device 1 and Device 2. The results of the quality factor measurements are listed in Table 5.5.

Table 5.5. The results of quality factor measurements.

Setup	-3dB Method	Port1	Device1	Port2	Device2	Tuners	Q_0	f_{res} (MHz)
0	S_{11}	Coupler	N-type converter	-	-	3	17260	800
1	S_{21}	The flange of beam pipe	Pick-up antenna	The flange of beam pipe	Pick-up antenna	no	19865	794.59
2	S_{21}	The flange of coupler	50 Ω loop antenna	The flange of tuners	50 Ω loop antenna	no	16492	794.89
3	S_{21}	Coupler	N-type converter	The flange of hole	Pick-up antenna	3	14760	800
4	S_{21}	The flange of coupler	50 Ω loop antenna	The flange of tuners	50 Ω loop antenna	2	14867	799.87
5	S_{21}	The flange of beam pipe	Pick-up antenna	The flange of beam pipe	Pick-up antenna	3	15038	800

The simulation results of quality factor are shown in Table 5.1. When we compare the simulation results from Table 5.1 with the measurement results shown in Table 5.5, differences are observed for each experimental setup. This difference is attributed primarily to the difference in the conductivity value of the material used in the simulation and the production. The following results are obtained when the simulation is performed again by using CST-MWS according to the conductivity of the material. This reduces the unloaded Q-factor to 22898 (21905) without (with) tuners, as seen in Figure 5.1.

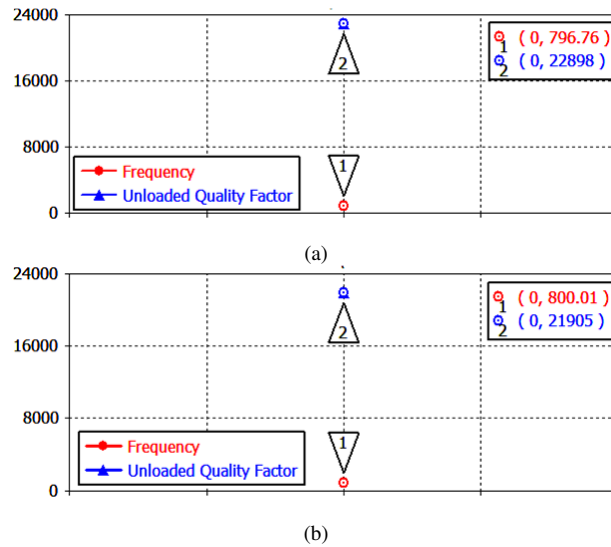


Figure 5.1. The resonance frequency and the unloaded quality factor of pillbox cavity for $\sigma = 2.510^7 S/m$ (a) without tuners, (b) with tuners

Yet there still remains a difference between measurement and simulation. According to Table 5.6, this percentage error is higher in the measurements taken with the tuners. The reason is attributed to fact that the tuners would cause more field perturbation and increase the conductance losses when they enter the cavity beyond a certain ratio.

Table 5.6. The percentage error between measured and simulated values

Setup Number	With Tuners Q_0	Without Tuners Q_0
0	21.2%	-
1	-	13.2%
2	-	27.9%
3	32.6%	-
4	32.1%	-
5	31.3%	-

To measure the quality factor in the transmission type method, the dimensions of the measurement points and antennas should be equal in order to increase the accuracy of the measurement as mentioned in Section 4.1.2. In this context, when the experimental setup 3 and setup 5 are compared, the effect of this situation is clearly seen. In addition, RF leakage, loss of the cables or surface roughness due to production may cause differences.

In order to determine the performance of transmission line, S_{11} parameter of the pillbox cavity and power coupler system was set to -40.195 dB to obtain full power transmission for the cavity without reflection. Then, the S_{21} parameter of the transmission line was set to -0.132 dB by adjusting the tuners to obtain maximum transmission. After the cavity and coupler system was connected to the transmission line, the system was tested with a specially designed power supply capable of delivering a fine adjustable 100Watt power running at 800MHz. The system has been observed to work successfully with the maximum value of the power source 112Watt and the reflected power is only 0.021% according to Table 4.2.

Consequently, the simulations and measurements related to the pillbox cavity and power coupler have been found to be consistent with each other. The performance of the transmission line indicated that it can be used for high power applications in accordance with the measurements. The use of a simple cavity structure provides a basis for future accelerator cavities and has provided new ideas and technical knowhow to the project staff about how to measure at high frequencies and how to improvise solutions to unexpected issues.

REFERENCES

- Alesini, D. (2011). Power coupling.
- Balanis, C. A. (2012). *Advanced engineering electromagnetics; 2nd ed.* John Wiley - Sons.
- Bermejo, F. and Sordo, F. (2013). Technical design report: Ess-bilbao rfq. *ESS-Bilbao Consortium Report Series, ESSB-Rep-2013-08.*
- Bray, J. and Roy, L. (2004). Measuring the unloaded, loaded, and external quality factors of one-and two-port resonators using scattering-parameter magnitudes at fractional power levels. *IEE Proceedings-Microwaves, Antennas and Propagation*, 151(4):345–350.
- Carter, R. (2011). Rf power generation. *arXiv preprint arXiv:1112.3209.*
- Caspers, F. (2012). Rf engineering basic concepts: the smith chart. *arXiv preprint arXiv:1201.4068.*
- Caspers, F. and Kowina, P. (2014). Rf measurement concepts.
- Çetinkaya, H., Çağlar, A., Çicek, C., Özbey, A., Sunar, E., Türemen, G., Yıldız, H., Yüncü, A., Özcan, E., Ünel, G., et al. (2018). Kahve laboratory rf circulator and transmission line project. In *AIP Conference Proceedings*, volume 1935, page 070002. AIP Publishing.
- Collin, R. E. (2007). *Foundations for Microwave Engineering.* John Wiley & Sons.
- Cooper, R. (1992). High power rf transmission.
- CST (2018). Computer simulation technology - microwave studio. accessed at July 2019.
- Degiovanni, A. (2018). Accelerating structures.

- Eberhardt, J. (2014). Investigation of quality factor of resonators. Technical report.
- Gerigk, F. (2011). Cavity types. *arXiv preprint arXiv:1111.4897*.
- Gerigk, F. (2013a). Radio frequency for accelerators. *Modern North Korea Studies*, pages 214–271.
- Gerigk, F. (2013b). Rf basics i and ii.
- Hinterberger, F. (2006). Electrostatic accelerators.
- Jensen, E. (2016). Rf cavity design.
- Jensen, E. (2018). Rf superconducting cavities-non-elliptical cavities.
- Jin, J.-M. (2015). *The finite element method in electromagnetics*. John Wiley & Sons.
- Kajfez, D. (1999). Q factor measurements, analog and digital. *University of Mississippi Dept. of Electrical Engineering*, www.ee.olemiss.edu/darko/rfqmeas2b.pdf.
- Kumar, R. (2017). High power rf coupler design for accelerator cavities. pages 20–22.
- Liao, S. Y. (1989). *Microwave devices and circuits*. Pearson Education India.
- MATLAB (2019). Matrix laboratory. accessed at July 2019.
- Nyfors, E. G. et al. (2000). *Cylindrical microwave resonator sensors for measuring materials under flow*. Helsinki University of Technology.
- Padamsee, H. (2015). Design topics for superconducting rf cavities and ancillaries. *arXiv preprint arXiv:1501.07129*.
- Pozar, D. M. (2012). *Microwave engineering; 4th ed.* Wiley.
- Rylander, T., Ingelström, P., and Bondeson, A. (2012). *Computational electromagnetics*. Springer Science & Business Media.
- Sadiku, M. N. (2000). *Numerical techniques in electromagnetics*. CRC press.

SOLIDWORKS (2018). Solid modeling computer aided design. accessed at July 2019.

Tenenbaum, P. (2003a). Fields in waveguides. *Multi-cell RF Cavity*, pages 1–62.

Tenenbaum, P. G. (2003b). A brief introduction to rf power sources.

Vretenar, M. (2016). Linear accelerators. *arXiv preprint arXiv:1601.05210*.

Wangler, T. P. (2008). *RF Linear accelerators*. John Wiley & Sons.

Wolski, A. (2015). Maxwell's equations for electrostatics.